FUSION SCIENCE AND TECHNOLOGY · VOLUME 75 · 886–917 · NOVEMBER 2019

DOI: https://doi.org/10.1080/15361055.2019.1610685

Critical Exploration of Liquid Metal Plasma-Facing Components in a Fusion Nuclear Science Facility

C. E. Kessel,[a,b]* D. Andruczyk,[c] J. P. Blanchard,[d] T. Bohm,[d] A. Davis,[d] K. Hollis,[e] P. W. Humrickhouse,[f] M. Hvasta,[a] M. Jaworski,[a] J. Jun,[b] Y. Katoh,[b] A. Khodak,[a] J. Klein,[g] E. Kolemen,[a] G. Larsen,[g] R. Majeski,[a] B. J. Merrill,[f] N. B. Morley,[h] G. H. Neilson,[a] B. Pint,[b] M. E. Rensink,[i] T. D. Rognlien,[i] A. F. Rowcliffe,[b] S. Smolentsev,[h] M. S. Tillack,[j] L. M. Waganer,[k] G. M. Wallace,[l] P. Wilson,[d] and S.-J. Yoon[f]

[a]*Princeton Plasma Physics Laboratory, Princeton, New Jersey*
[b]*Oak Ridge National Laboratory, Oak Ridge, Tennessee*
[c]*University of Illinois, Campaign-Urbana, Illinois*
[d]*University of Wisconsin, Madison, Wisconsin*
[e]*Los Alamos National Laboratory, Los Alamos, New Mexico*
[f]*Idaho National Laboratory, Idaho Falls, Idaho*
[g]*Savannah River National Laboratory, Jackson, South Carolina*
[h]*University of California, Los Angeles, Los Angeles, California*
[i]*Lawrence Livermore National Laboratory, Livermore, California*
[j]*University of California, San Diego, San Diego, California*
[k]*Consultant, 10 Worchester Court, O'Fallon, Missouri*
[l]*Massachusetts Institute of Technology, Cambridge, Massachusetts*

Received June 1, 2018
Accepted for Publication April 18, 2019

Abstract — *Liquid metal (LM) plasma-facing components (PFCs) may provide a resolution to the challenging fusion environment, particularly the first wall and divertor surfaces. Transforming these concepts into viable technologies will require considerable research and development. With the fusion nuclear regime in mind, the Fusion Energy System Studies group examined LM PFCs in order to identify needed research thrusts that could accelerate their development and assess their viability. Liquid metal behavior, solid substrate aspects, and fusion facility integration aspects are examined, with concepts as the research focusing element. The concepts applied to a fusion nuclear device are the primary definer of the LM parameters, environmental conditions, and operational aspects. This forms the research strategy recommended for these complex systems.*

Keywords — *Liquid metals, plasma-facing components, Fusion Nuclear Science Facility, design, tokamak.*

Note — Some figures may be in color only in the electronic version

I. INTRODUCTION

The development of long-lifetime plasma-facing components (PFCs) provides a significant barrier to the success of fusion energy. These materials will see both high-energy neutrons from the plasma and high plasma and neutron fluxes to their surfaces. The associated heat and particle fluxes as well as volumetric heating will give rise to material evolution and high temperatures with significant gradients. Nuclear damage and transmutation production are maximum at the plasma-facing surface. Plasma exposure will erode and reconstitute the surface materials (through

*E-mail: kesselce@ornl.gov

redeposition and migration). The application of a liquid layer for the PFC has the potential to alleviate some of the extreme conditions a solid PFC would need to endure. This paper reports on the examination of liquid metal (LM) PFCs in the Fusion Nuclear Science Facility[1] (FNSF), and accompanying papers will provide detailed assessments in specific areas.[2–8] The study is roughly separated into four areas: (1) LM characteristics, (2) solid substrate characteristics and interactions, (3) integration issues associated with these LM PFCs, and (4) specific first wall (FW) and divertor concepts. For this activity the LM PFC is taken to be added on top of an otherwise conventional breeding blanket and/or in the divertor and therefore is relatively thin, ≤2.5 cm. The actual thickness of the LM layer will be determined by a number of trade-offs in the design of the concept [e.g., magnetohydrodynamic (MHD), heat transfer, exposure distance, capillary]. The LM will require a solid substrate. The LM PFC will introduce another fluid system into the fusion core in addition to the main coolant He and breeder PbLi; the dual-coolant lead-lithium (DCLL) blanket used in the FNSF is assumed.

The primary reasoning as to why to consider a liquid layer on the plasma-facing surfaces includes the following:

1. to eliminate plasma degradation of a solid PFC (erosion, reconstitution) as a lifetime limit
2. to remove the surface heat load that would happen with a solid PFC
3. to reduce the nuclear damage and transmutation that would happen with a solid PFC
4. to reduce the largest gradients (damage, temperature, stress) that would happen with a solid PFC.

In general, it is understood that a LM layer would accomplish all of these and is the main motivation to examine their potential. Different concepts, such as flowing or capillary, would accomplish this to differing degrees primarily due to differing thickness of the liquid layer and what the liquid material is. This study is intended to identify what critical research and development (R&D) is needed to understand the LM behavior in the fusion environment, how specific concepts apply in a FNSF, and steps to confirm the credibility of LM as a PFC in a reasonable time frame. This can be contrasted with previous activities targeting large neutron and surface heat fluxes as their goal.[9,10] Numerous reviews and progress reports have been made recently in the area of LM PFCs (Refs. 11, 12, and 13), although these are not exhaustive, that span experimental facilities, concepts, and facilities where LMs or PFC surface coatings are applied. Since the LM PFC area is still immature and results are evolving, major issues are identified that require resolution in the appropriate prototypical fusion environment.

The primary goal of research in the LM PFC area is to develop a technical basis for a practical system that can be applied to a fusion device. The prospect of using LMs as PFCs requires a series of R&D activities that can establish the viability of this approach and to do it in an expedient way. Although one can answer "yes" to the potential benefits of a LM layer on solid substrates in a fusion device, posed earlier, the viability of a workable LM system remains unknown. This unknown presents a significant barrier to adopting LMs as the solution to the challenging PFC problem in fusion. However, establishing a focused program on resolving issues and uncertainties with an eye toward integrated and prototypical systems is the motivation of this paper and study into LM PFCs. In this context the LM PFC issues are opportunities, and they remain issues only until we resolve them or circumvent them.

II. LIQUID METAL PROPERTIES

Liquid metals have several properties that require attention when applying them to plasma-facing surfaces. The low-melting-point metals in the periodic chart can be scanned for their vapor pressure (evaporation rate) and nuclear responses as well as a number of other properties. Most of these metals can be rejected based on the evaporation rates over temperature ranges of interest (~350°C to 800°C), leaving Sn, Sn-Li, Ga, Ga-Li, In, In-Li, and Pb-Li. Lithium is also retained for operation at the lower-temperature range or in a high-evaporation regime, and Pb-Li is retained for comparison due to its high breeding potential and blanket application. The evaporation rates are shown in Fig. 1 for the candidates, although In-Li and Ga-Li data are not available. The evaporation rates for Pb-Li and Sn-Li are determined using activity coefficients from Ref. 14. Phase diagrams exist for Sn-Li (Ref. 15), Pb-Li (Ref. 16), and In-Li (Ref. 17), all showing similar trends with low melting temperatures at the lower Li concentration range and higher melting temperatures and multiple intermetallics at the higher Li concentration range. The phase diagram for Ga-Li (Ref. 18) shows different behavior, with a rapidly rising melting temperature with increasing Li content at lower Li content range (e.g., 500°C at 20 at. % Li) and a falling melting

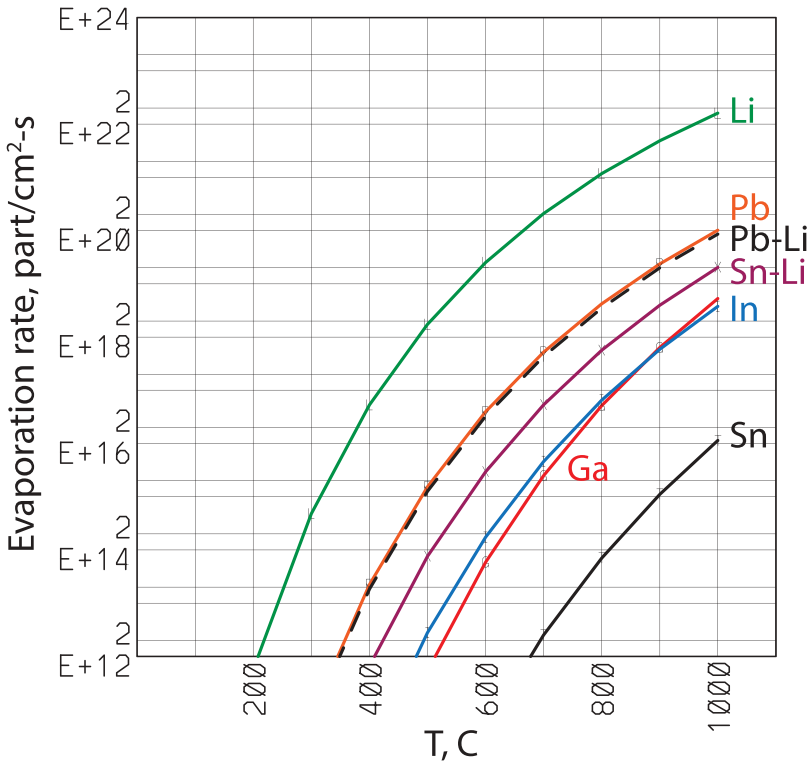

Fig. 1. Evaporation rates for some LM PFC candidates.

temperature with rising Li content at the higher Li content range (e.g., 260°C at 90 at. % Li). Appropriate levels of Li in Sn-Li range from a few to 25% before the melting temperature rises rapidly, while in In-Li, the Li level might range from a few to 15%. Pb-Li has a eutectic (minimum melting temperature over constituency range, except 100% Li) concentration around 15.7% Li and 84.3% Pb (forming a V liquidus line in the phase diagram), which restricts practical operation to avoid solidification and intermetallic formation due to a rapidly rising melting temperature on both sides of the eutectic composition. From the application point of view, any LM must be operated well above its melting point ($T - T_{melt} > 50$°C to 100°C) since it must travel through an entire loop including the plasma chamber, tritium extraction, heat exchanger (HX), and cleanup while avoiding any solid precipitation (except possibly in the cleanup system).

The operating temperature of a LM in the plasma chamber and subsequently in the overall loop in a fusion facility is dictated by its evaporation rate (and other losses), intrinsic impurities in the LM, impurities introduced into the LM by corrosion, the heat load it receives and speed that it flows through the plasma chamber, and subsequent materials it interfaces outside the fusion core. This can be complicated by the introduction of large fluxes of hydrogen to the LM while in the plasma chamber, possibly affecting its constituency and properties. The requirements of these external apparatuses (e.g., tritium extraction) may provide additional constraints. For example, the technique for tritium extraction from a LM may be compromised by other impurities in the LM, requiring that they be removed in advance. The attractiveness of a LM PFC for thermal energy conversion is determined by the maximum achievable temperature.

Because Ga and In are elements that are recovered only from the mining and purification of other materials, Al, Zn, and Cu, for example, they are not mined directly since they are so dilute in the earth's crust. The by-product recovery of these elements has been sufficient for industrial applications; however, requiring the recovery of a ton or more for each fusion power plant would require ramping up the mining of other metals. In addition, Ga has very aggressive corrosion of steels, including ferritic steels like reduced activation ferritic martensitic (RAFM) fusion steel. For these reasons the use of Ga and In or their alloys will no longer be considered, reducing the list of considered LMs to Li, Sn, Sn-Li, and Pb-Li.

II.A. Loss Rate from LM Surfaces

The loss rate from a LM layer in the plasma chamber plays a central role in its viability and operating temperature range. The physical sputter,[19–21] ad-atom,[22–26] and evaporation combination model is taken as the basis for determining this loss flux and can be given for Li by (for example)

$$\phi_{loss}^{\mathrm{Li}} = f_{neut}[\Sigma_j \phi_{\mathrm{D}}(E_j) Y_{\mathrm{D,Li}}(E_j) + \Sigma_j \phi_{\mathrm{T}}(E_j) Y_{\mathrm{T,Li}}(E_j) + \Sigma_j \phi_{\mathrm{He}}(E_j) Y_{\mathrm{He,Li}}(E_j) + \Sigma_j \phi_{\mathrm{Li}}(E_j) Y_{\mathrm{Li,Li}}(E_j) + \Sigma_j \phi_{\mathrm{Z}}(E_j) Y_{\mathrm{Z,Li}}(E_j)] + f_{neut}^{ad} \times \{\Sigma_j \phi_{\mathrm{D}}(E_j) Y_{\mathrm{D,Li}}^{ad}(E_j) + \Sigma_j \phi_{\mathrm{T}}(E_j) Y_{\mathrm{T,Li}}^{ad}(E_j)\} / (1 + A\exp(E_{eff}/kT)) + \phi_{evap}^{\mathrm{Li}}(T) \ ,$$

where

$\phi_{\mathrm{D,T,He,Z,Li}}$ = particle flux onto the LM (particle/$\mathrm{m^2 \cdot s^{-1}}$)

Y = yield in atoms/ion or atoms/atom

f_{neut}, f_{neut}^{ad} = fraction of loss particles that are neutral (since charged particles are most likely returned to the surface within the sheath)

Y^{ad} = ad-atom yield (atom/ion)

A, E_{eff} = parameters for the ad-atom process

$\phi_{evap}(T)$ = normal thermal evaporation flux, given by $CP_{vap}(T)/(\mathrm{mT})^{1/2}$.

The physical sputtering terms include D and T hydrogen ion, He ion, Li ion, and other impurity (Z) ion bombardment, although the ad-atom loss is only shown for the hydrogen species bombardment. The summations are over the incident particle energies (energy groups). The ad-atom process involves a particle flux that excites near-surface atoms to reside on top of the surface where they undergo thermal evaporation. This is dependent on the flux (which provides the production of ad-atoms) and the impinging particle's energy (lower is more likely to produce ad-atoms due to shallow energy deposition). Both the fluxes to the surface and the yields are energy dependent. In general, ions hitting the surface would be perpendicular due to the sheath, while neutral particles can impinge from any angle. The emitted particles would also have some initial angular distribution. These angular dependences are suppressed in the loss equation shown above for clarity. This loss formulation is illustrated in Fig. 2, for Li, one of the few materials where the ad-atom parameters have been estimated.[24,25] Here, we use A = 1E–7, E_{eff} = 0.9 eV, $Y_{\mathrm{D,Li}}$

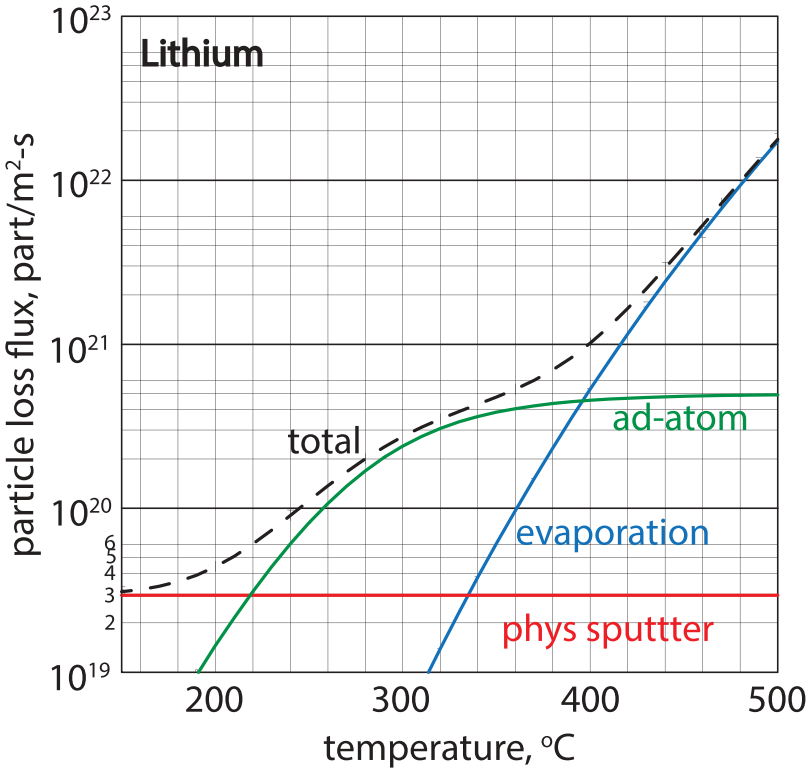

Fig. 2. Loss from lithium LM as a function of temperature from physical sputtering, ad-atom loss, and evaporation. This assumes specific ad-atom coefficients.

= 0.1, $Y_{T,Li}$ = 0.1, $Y_{He,Li}$ = 0.16, $Y_{Li,Li}$ = 0.3, $Y_{Z,Li}$ = 0, f_{neut} = 0.35, f_{neut}^{ad} = 1.0, Y^{ad}/Y^{ps} = 50 (ratio of ad-atom yield to physical sputtering yield), $\phi_D = \phi_T = 0.5 \times 10^{20}$/m^2·s, $\phi_{He,Li}$ = 0, and $\phi_{Li} = 0.65 \times 10^{20}$/m^2·s. The physical sputtering provides a constant loss term, and the evaporation rate grows continuously with temperature, while the ad-atom loss rises earlier than the evaporation and can lead to a higher loss rate at lower temperatures. The hydrogen fluxes used in this example were determined by two-dimensional (2-D) scrape-off-layer (SOL) plasma simulations for the FNSF (Ref. 27) but may not be self-consistent with a Li plasma-facing material. In general, most physical sputter yields are available for liquid Sn (Ref. 20), Li (Ref. 19), and Sn-Li (Ref. 21), although the lower-energy range (<200 eV) lacks data and TRansport of Ions in Matter (TRIM) analysis has been used to fill in this region. Evaporation data are widely available. The ad-atom physical parameters are motivated and simulated in Refs. 24 and 25 but are still generally fit to the data and are barely available experimentally. Figure 2 illustrates the importance of characterizing the ad-atom loss channel since at a given allowable flux of particles lost from the LM surface, there is a maximum temperature of operation. From previous results with 2-D SOL simulations for lithium,[28] it was determined that a net loss flux of 2×10^{20} Li particles/m^2·s could be tolerated before diluting the core plasma too heavily. Based on evaporation only, the maximum operating temperature for lithium would then be about 380°C, while including the ad-atom model could make this less than 300°C. Relatively small variations in these parameters can make this loss channel important or unimportant. A recent study with thin Li layers in MAGNUM-PSI indicates that the loss model requires modification due to the formation of LiH under high hydrogen fluxes, which would have different properties from Li (Ref. 29). More detailed information on the energy distribution of the impinging ions and neutrals and on the sheath acceleration, redeposition, ionization, and overall near-surface physics is also needed to complete a model for losses.

II.B. Core Plasma Tolerance for LM Species

The tolerance of the core plasma for LM impurities is largely driven by fuel dilution, core plasma radiation, Z_{eff} limitations, and the need to meet heat flux limits in the divertor and minimum neutron wall loads. A coronal equilibrium model is used here,[30] and radiation losses include cyclotron, bremsstrahlung, and line. The fraction $f_X = n_X/n_e$. For Li (Z = 3), the FNSF had no operating space since Li does not radiate in the core plasma and the divertor heat load constraint could not be met or the fuel was diluted so much that the neutron wall load target was not met. If Ar (Z = 18) was introduced with Li, then solutions ranged from f_{Ar}/f_{Li} = 0.003/0.02 to 0.0045/0.015. If Sn (Z = 50) was introduced with Li, then the solutions ranged from f_{Sn}/f_{Li} = 1.5E–4/0.037 to 5.5E–4/0.027. For Sn by itself, the maximum fraction in the core plasma was 6.0E–4 and was limited by a maximum Z_{eff} of 2.5, which is used as a limit since the lower hybrid (LH), ion cyclotron (IC), and electron cyclotron (EC) current drive efficiencies scale as $1/(C + Z_{eff})$. This Z_{eff} limit determined the maximum Ga (Z = 31) to be 1.7E–3 and the maximum W (Z = 74, used for comparison) to be 2.6E–4. From these limits one can estimate the tolerable loss flux from the LM by scaling, $\phi_{LM1,loss}^{max}$ to $\phi_{LM2,loss}^{max}$ $(Z_1/Z_2)^2$, although this should not be used for Li since it does not radiate from the core plasma. The tolerable fraction of LM (e.g., $f_{Sn} = n_{Sn}/n_e$) in the core plasma implies a separatrix density, determined by the density profile. Tables I and II show the various cases along with other parameters for the FNSF plasma. The maximum values for the impurities in the core plasma can vary depending on the detailed profiles and particle transport, so these can be considered approximate. The analysis of the SOL and divertor can establish a separatrix density for a given flux source coming from the wall, similar to what is done in Ref. 28. The possible segregation of Li to the surface of LM alloys M-Li indicates that these materials may only release Li while providing a high recycling wall condition, unlike pure Li, which would release Li and have a low recycling wall condition. This is discussed further in Sec. II.C. From the evaporation rates shown in Fig. 1, it is clear that Li has a much higher rate than the M-Li alloys.

II.C. Segregation of the Low Surface Tension Constituent in a LM Alloy

The segregation of one constituent to the surface of a LM in an alloy (M-Li) is driven by the surface tension, and the constituent with the lower surface tension will move to the free surface. This is not a large-scale separation of the two components but only involves several monolayers near the surface while the bulk LM retains the stoichiometry of the alloy (e.g., 80% Sn and 20% Li). There are other forms of segregation, such as gravity in the case of heavy and light components, but this will not persist if the LM layer is not flat with the surface facing upward and stagnant. The physics of surface tension and segregation has been studied outside of fusion for some time. A particularly good theoretical analysis of segregation for NaK LM is given in Ref. 31, using a detailed variational construction and a density profile trial

TABLE I

Acceptable Lithium and Argon, or Lithium and Tin Impurity Fractions in the FNSF Core Plasma

Ar Fraction	0.003	0.0035	0.004	0.0045	0.005
f_{Li}^{max}	0.02	0.02	0.018	0.015	0.01
P_{fusion} (MW)	509	505	512	505	502
$P_{rad,core}$ (MW)	49	56	60	67	77
Z_{eff}	2.09	2.25	2.37	2.51	2.81
$H_{98(y,2)}$	0.99	1.0	1.0	1.02	1.01
$<N_W>$ (MW/m^2)	1.18	1.16	1.18	1.15	1.16
f_{DT}	0.84	0.83	0.84	0.82	0.82
Sn fraction	0.00015	0.00025	0.00035	0.00045	0.00055
f_{Li}^{max}	0.037	0.035	0.034	0.029	0.027
P_{fusion} (MW)	505	505	502	502	509
$P_{rad,core}$ (MW)	49	70	84	102	116
Z_{eff}	1.63	1.88	2.11	2.34	2.57
$H_{98(y,2)}$	0.99	1.0	1.02	1.02	1.04
$<N_W>$ (MW/m^2)	1.15	1.16	1.16	1.17	1.16
f_{DT}	0.84	0.84	0.83	0.83	0.84

TABLE II

Acceptable Tin, Gallium, Argon, and Tungsten Impurity Fractions in the FNSF Core Plasma

	Sn (Z = 50)	Ga (Z = 31)	Ar (Z = 18)	W (Z = 74)
f_{Li}^{max}	0.0006	0.0017	0.0049	0.00026
P_{fusion} (MW)	516	536	516	560
$P_{rad,core}$ (MW)	115	72	63	186
Z_{eff}	2.53	2.45	2.50	2.46
$H_{98(y,2)}$	1.02	0.99	1.00	1.03
$<N_W>$ (MW/m^2)	1.19	1.23	1.19	1.28
f_{DT}	0.91	0.90	0.87	0.93

function. This analysis shows the density profiles for Na and K in the vicinity of the LM surface, clearly showing the K density exceeding that of Na on the surface over a range of fractions of K in Na, and even as the fraction of K drops very low (~2%), the K is localized to the surface and has equal density as Na. This reference also shows how the segregation is diminished as the temperature rises. A strong experimental reference is Ref. 32, where a significant reduction in surface tension with segregation is observed with Sn added to Cu or Ag and where a thermodynamic formulation, with Butler's equation, is used to estimate the surface tension and segregation properties. This phenomenon is evident in many alloy systems and has been suggested for Sn-Li (Refs. 33 and 34); however, a detailed understanding will be needed to project the performance of this alloy to fusion conditions. Interesting and potentially beneficial properties have been observed or postulated for Sn-Li including (1) Sn does not appear to be physically sputtered, only Li (Ref. 21); (2) self-sputtering of Sn reaching unity is avoided[21]; (3) uptake of hydrogen is limited[35] unlike pure Li; and (4) Sn-Li has a much lower evaporation flux than Li. Concerns with establishing and sustaining the segregation effect include (1) weakening with increasing temperature, (2) the speed with which this segregation is established versus mixing or other fluid disturbances, (3) formation of LiH in the segregated layer, and (4) how impurities in Sn-Li could affect the segregation. Meanwhile, Pb-Li appears not to form a segregated Li surface or forms only a weak one.[36] Earlier work[37] had confused gravitational segregation with surface tension segregation, which is pointed out in Ref. 36. The surface tensions of Pb, Sn, Li, In, and Ga are shown in Fig. 3 along with Pb-Li.

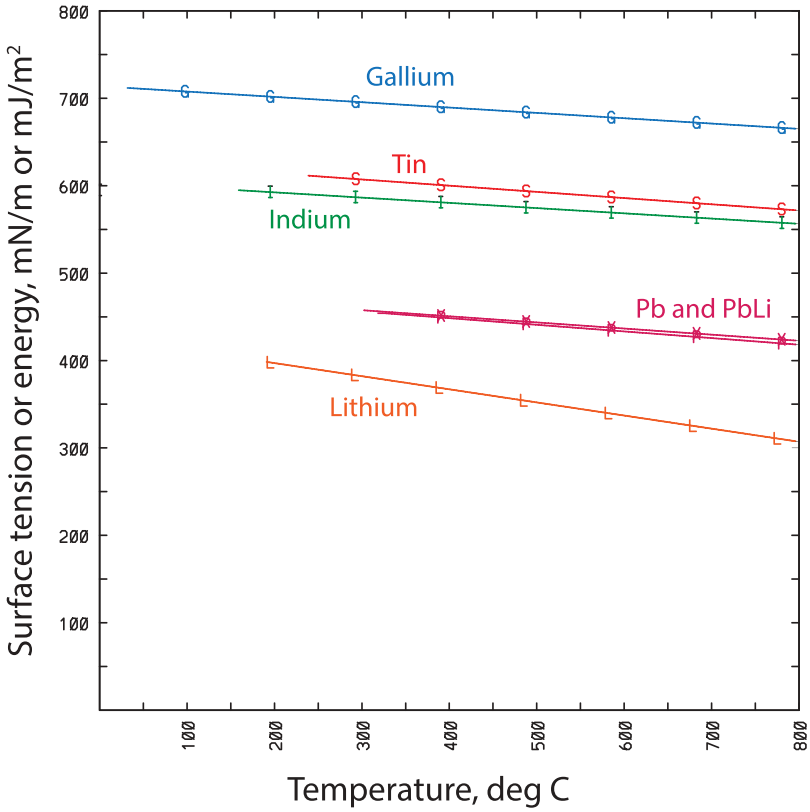

Fig. 3. Temperature dependence of the LM surface tension above their melting temperature for various LMs.

II.D. Lithium-Hydrogen Phase Diagram

The Li-H (Li-D and Li-T) interaction is critical in a fusion reactor where large fluxes of hydrogen will contact the LM regardless of the particular concept used, either on the FW or the divertor, although the fluxes can be quite different in these two regions. For LMs (e.g., Sn, Sn-Li, Pb-Li) other than Li, the interaction appears much weaker since their hydrogen solubilities are considerably lower than pure Li, although this requires more detailed confirmation. The Li-H or Li-LiH phase diagram (T versus composition) can be found in Refs. 38 and 39 while pressure versus composition can be seen in Refs. 40 and 41 with the full data accumulation for Li-H, Li-D, and Li-T in Ref. 42. The phase diagram, temperature versus hydrogen fraction shown in Fig. 4, shows six major regions: (1) the solid Li and solid LiH at $T < 180$°C; (2) the lower hydrogen content (Sieverts region), liquid Li from $T > 180$°C; (3) the liquid Li and solid LiH, $T < 685$°C to 690°C, and H fraction > solubility limit; (4) the liquid Li and liquid LiH, $T > 685$°C to 690°C, and H fraction > solubility limit or H fraction < upper solubility limit; (5) liquid LiH with very low Li, $T > 685$°C to 690°C, H > upper solubility limit; and (6) liquid Li and H, $T > 960$°C to 1000°C, where LiH decomposes. Apart from avoiding solidification of a Li-LiH LM solution, the all-solid region is not of interest. Above the melting temperature of Li, there is the lower hydrogen content region in which Li is a liquid and either hydrogen is dispersed in the liquid or LiH is dispersed in the liquid (region 2). In this region adding hydrogen to liquid Li can continue until the solubility limit is reached with hydrogen remaining in solution, after which adding more hydrogen LiH will precipitate out as a solid in solution if $T < 685$°C (region 3) or as an immiscible (does not mix) liquid if $T > 685$°C (region 4).

Assuming a flowing Li FW concept and that all impinging hydrogen is held up, one can calculate if the Li will reach the solubility limit while in the plasma chamber as a function of the thickness, flow speed, and temperature. This is shown in Fig. 5 for three different particle fluxes ranging from 10^{23} to 10^{25} particles/m^2·s for a flow length of 0.76 m typical of a divertor surface in the FNSF. Flow speeds range from 1 to 10 m/s, and the LM layer thickness ranges from 1 to 10 cm. The higher particle fluxes and lower flow speeds lead to the highest hydrogen concentration and depending on the

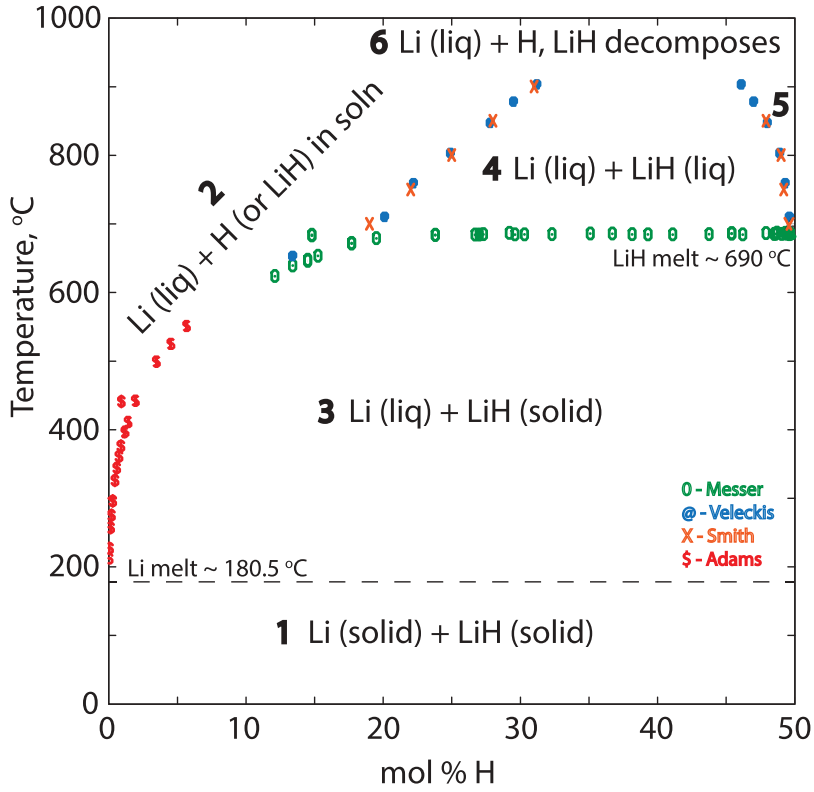

Fig. 4. Phase diagram data for Li-H (Li-LiH), from Messer et al.,[43] Veleckis et al.,[40] Smith et al.,[41] and Adams et al.[38]

temperature can exceed the solubility limit and lead to LiH precipitation (region 3). The hydrogen particle fluxes are lower on the FW than in the divertor, and even though the flow paths tend to be longer (5 to 8 m) than in the divertor, the uptake of hydrogen did not reach solubility limits. It is important to note that the low flow speeds (<1 m/s) and thin LM layers (<1 cm) will lead to the greatest potential for hydride formation and precipitation under the assumptions of this model. Concepts that have very thin layers and very slow flow (not shown on the graph in Fig. 5) could be susceptible to this effect. The formation of solid LiH in solution can lead to deposition on solid surfaces along its flow path, including outside the plasma chamber on various manifolding. It is not known that every incident hydrogen (ion, atom, or molecule) will remain in the lithium, and this will depend on several factors such as the hydrogen energy, the environment (plasma or gas), and the LM (temperature, motion). Hydrogen uptake is discussed further in Sec. II.F.

The region with the hydrogen content exceeding the solubility limit, with $T < 685$°C, is a combination of liquid lithium with hydrogen in solution and solid LiH. In a working system of a LM PFC, the presence of a solid in solution can lead to precipitation out onto solid substrate or piping surfaces. Meanwhile, the temperature range of liquid Li has typically been set roughly at <400°C due to high evaporation rates, where the solubility limit of hydrogen is about 1.2 at. %. In this region extending from $T \sim 180$°C to 900°C, when the hydrogen is less than the solubility limit, does Li with H in it evaporate at the same rates as pure Li? Furthermore, when the hydrogen content exceeds the solubility limit, is the Li evaporation rate the same or different from pure Li? The Li evaporation rate could simply be a weighted value based on the amount of free Li in the Li-LiH mixture. Understanding the properties of the Li-LiH mixture is needed to properly assess evaporation rates and the operating temperature range as well as solid precipitation potential. The presence of LiH could significantly alter other processes including physical sputtering and ad-atom losses, wetting, and segregation. There may even be a higher-temperature operating regime for a LM mixture of Li and LiH, for example, ~800°C to 1000°C, where Li and LiH are liquids or where Li and H coexist. This would be dependent on the evaporation rates in these regimes. For example, evaporative divertor concepts like the vapor box divertor concept[44–46] rely on lithium operating at ≥700°C, where evaporation is very strong, decreasing to ~300°C, across the divertor length, where condensation should dominate over evaporation.

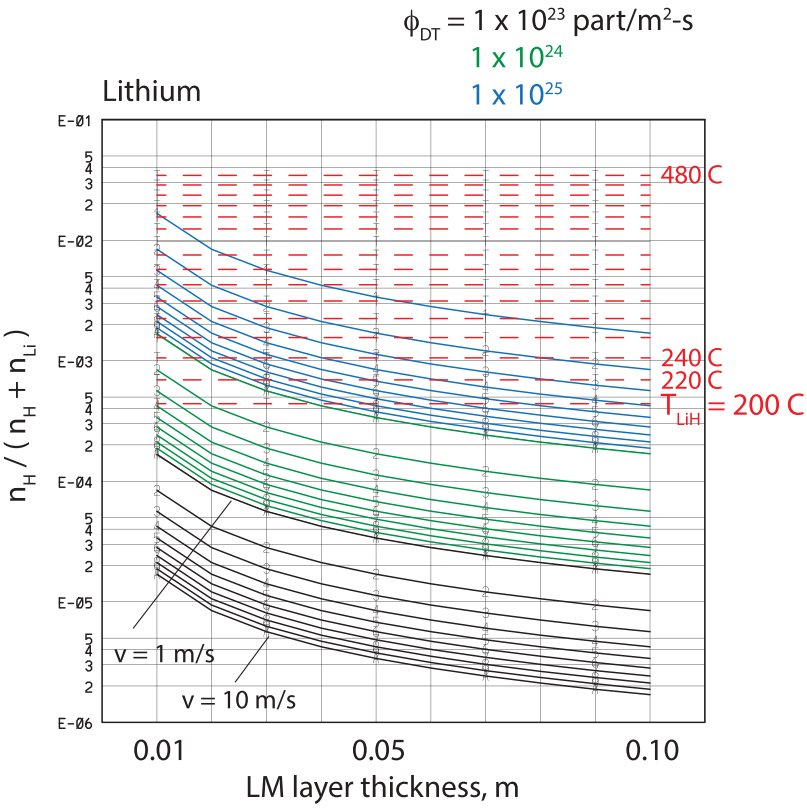

Fig. 5. Variation of the hydrogen fraction in Li-H as a function of LM thickness and flow speed, and D-T particle flux to the Li surface. Solubility limit is noted by dashed lines for various temperatures.

The different regions of the divertor would be in different regions of the phase diagram depending on their operating temperature, pressure, and hydrogen concentration. These factors would likely impact the lithium interaction with hydrogen.

II.E. Wetting of LMs on Substrate Materials

Wetting of a solid surface by a liquid refers to its ability to adhere to the surface and directly reflects an interaction between the liquid and solid. This property is measured by a contact angle, often experimentally measured with a drop of liquid on a surface or a solid plate dipped and removed from a liquid bath. This angle is between the solid surface and the liquid surface at the contact point, with >90 deg referred to as poor wetting and <90 deg referred to as good wetting. Wetting is strongly complicated by practical features of the liquid and the solid. Surface roughness, solid constituents, solid impurities, liquid constituents, liquid impurities, temperature, and time all contribute to the final wetting behavior.[47–50] Here, the difference between a high-purity laboratory measurement and an industrial LM flow system is tremendous. Wetting has also been studied outside fusion extensively with some applications being underground oil wetting of rock, soldering, coatings, bonding metals to ceramics, brazing and joining, melting and casting, and construction of composite materials. Good wetting is fundamental to capillary LM concepts, both in feeding the LM from a reservoir to the plasma-facing surface but also for adhesion of the LM to the substrate surface, which is often a mesh or nonsmooth structure. One of the most important aspects of wetting is the interaction between the LM and the substrate material, which tends to enhance wetting. For example, the formation of interlayers between the solid substrate material and the LM can substantially improve wetting, even for systems that originally had poor wetting.[49] This was observed to occur over time with the duration shortened by higher temperatures. In addition, the interlayers were different based on impurities in the solid substrate. These phenomena are interconnected with corrosion.[50] A recent experiment on wetting of liquid lithium on several materials as a function of temperature[51] showed the impact of surface conditions and that Li wets itself very well (it is well known that a material will wet itself). Excepting capillary systems, why does wetting matter? For flowing LM systems, is wetting actually important? Theoretical

work in Ref. 52 examines the impact of finite slip, associated with poor wetting, at the conduit walls in duct flow, and found that this condition led to less drag and lower projected pressure drops. The implications for free-surface flow have not been analyzed. Heat transfer examinations in Ref. 53 indicate that the convective heat transfer coefficient was reduced by only 10% in a finite slip situation compared to the typical no-slip condition. In a fusion reactor, which is really an industrial-scale system, a LM PFC system may transiently experience mediocre wetting; however, the inevitable interactions like corrosion or infiltration could improve wetting quickly, depending on the material substrate. In fact, this is a common observation for sodium (Na) flow in ducts[54] where the observed flow velocity is higher initially when oxide layers are present inside of piping, but the velocity drops as the oxide layer is worn off and the Na wets the pipe walls because it is interacting with the pipe wall material. Wetting studies will need to move past basic studies and approach the prototypical conditions to make relevant conclusions for LMs in fusion devices.

II.F. Hydrogen Uptake in LMs

The uptake of hydrogen (D and T) by a LM inside the plasma chamber as the LM is in contact with the SOL and divertor is important in order to understand its impact on plasma operation as well as its handling for tritium outside the fusion core. It is well known that lithium can retain hydrogen up to 1:1 Li:H ratio[55] and that uptake from a plasma environment can be very strong. Since the mobility of hydrogen is high in liquid lithium, hydrogen can continue to be absorbed up to this limit of one hydrogen atom per lithium atom. Recent experiments on thin films of Li on MAGNUM-PSI (Ref. 29) indicate that this is a credible scenario, and it was necessary to reformulate loss analysis to consider LiH as a significant fraction of the exposed LM. As mentioned in Sec. II.D, thin Li films that move slowly could be particularly susceptible to hydriding. Whether every incident hydrogen ion or atom is retained in Li is under examination at present and appears to be drawing contradictory conclusions. Reference 55 indicates that hydrogen can be taken up to 1:1 ratio with lithium in plasma exposures, while gas experiments[56–58] have identified very small or no uptake. The features contributing to these differing results include (1) gas or plasma exposure and particle energy; (2) temperature range of exposure and follow-on hydrogen recovery with the possibility for high Li evaporation rates; (3) possible presence of oxygen; (4) thin layers or thick Li layers; (5) LiH surface formation, rapid hydrogen migration in Li, and agitation. The prototypical environment is also not fully established; for example, a plasma exposure is not a true vacuum in spite of low pressures since it involves impinging particles (ions and atoms) and not thermal gaseous species. However, the fluxes and energies of the ions and atoms in a plasma exposure need to be defined to much higher precision to better understand their impact.

There are several reports of the positive effects of lithium on plasma-facing surfaces in confinement devices for the performance of plasmas. Most of these are associated with a pumping effect of the SOL by the lithium[59–63] and subsequent changes in the edge plasma conditions. A recent report indicates that in the particular case of Li on carbon surfaces, Li may not be acting as the absorber of hydrogen[64] but that actually oxygen is providing the hydrogen uptake. Careful attention to the surface chemistry is critical to uncover the plasma and PFC interactions.

Several experiments have been performed to determine uptake of hydrogen by Li, using thermal desorption after a Li sample is exposed to hydrogen gas or plasma,[56,57] which can be complicated to interpret. It appears that the difficulty with virtually all of these experiments is likely the presence of oxygen. Even extremely small amounts of water can bring in a level of oxygen sufficient to alter the chemistry at the surface and near-surface layers of liquids and solids. The presence of Li_2O and LiOH at the surface of bulk Li or LiH creates chemical reactions that cause desorption of hydrogen at temperatures that would be hard to understand based on the phase diagram of Li-H alone.[65] Reference 65 shows the chemical reactions that are likely responsible for the observed desorption of hydrogen from Li and LiH samples, which actually involve LiOH, Li_2O, Li, and H. This will require further investigation to understand the role of impurities like O in the Li and H interactions.

The deuterium uptake was measured in Ref. 35 for Sn and SnLi using LM samples exposed in the ISSTOK tokamak. The apparatus was carefully constructed to allow preparation of the samples and plasma exposure within the same enclosure, controlling the impurities on the sample surfaces. Nuclear reaction analysis was used rather than thermal desorption and indicated that retention fractions ($n_D^{retained}/n_D^{incident}$) were approximately 3×10^{-4} for Sn and 2×10^{-4} for SnLi, showing very low retention typical of solid PFCs like tungsten.

II.G. Impurities in LMs

Impurities are a common occurrence in LMs, and they are normally separated into intrinsic impurities and extrinsic impurities. The former generally arise from the mining or recovery of the ore, processing of the material, and also the tendency of the LM to absorb environmental elements from air in the process of use or preparation, for example. Lithium has well-known primary intrinsic impurities of O, C, and N. Extrinsic impurities would be those introduced in a specific application, such as corrosion products from interactions with the substrate materials, plasma species (D, T, He, Ar, etc.), piping materials, and HX materials. Impurities in LMs can alter their behavior and properties significantly, such as wetting, segregation, and surface tension. For example, although corrosion of steels by Li is weak, this is only true if the N level is kept below 10 to 50 parts per million by weight (Ref. 66). For values above this, the corrosion can rapidly become more aggressive. At present, the International Fusion Materials Irradiation Facility (IFMIF) fusion neutron source development[67] applies Li on a large scale. Here, the Li loop, which does not have a magnetic field, has been devised to have a significant cleanup system to remove N, O, and C as well as tritium. One of the few examples of detailed impurity identification is done in Ref. 68 for the alloy Sn-Li as part of an effort to fabricate this alloy for use in research. It is important for the LM PFC community to begin characterizing the LM composition, particularly the impurities in these LMs, on a routine basis. Early studies in LMs during the 1950s and 1960s were plagued by different impurity contents among LM experiments, making the correlation of results very difficult. Naturally, this includes surface contamination in a wide range of experiments with free-surface LMs.

The corrosion products in a LM can be picked up in the piping or other apparatus (HX) outside the fusion core or in the fusion core. The impurities present in the fusion core will be exposed to neutrons and can experience transmutation to new radioactive impurities. Ultimately, the various impurities in the LMs must be removed with specific cleanup approaches. Knowledge of the corrosion products produced and their concentrations in the LM loop, including the plasma-facing part, is important to predict the various species present and devise cleanup techniques to remove them. At least initially knowing the solubility data for the various impurities in the LM is critical to understanding their tendency to remain in solution or precipitate out, as well as the temperature dependence of this behavior. However, there are many compounds that can form in the LM among the various impurities, complicating the treatment significantly. An interesting example of the complex impurity issues can be seen in Ref. 69, where the LM Hg is used as a target in a spallation neutron source and must deal with the wide range of impurities produced by nuclear reactions as well as the intrinsic impurities in the Hg, their subsequent behavior in the system, and finally their removal by techniques that are known in some cases and undeveloped in others. Once the chemistry of the impurities is understood, there may be motivation to remove specific impurities from the LM or their sources from the LM loop in order to avoid severe issues with its behavior.

III. NUCLEAR ASPECTS OF LM CANDIDATES

The plasma-facing LM will experience the direct neutron flux from the plasma, and its impact on tritium breeding is critical. Initially, a wide range of LMs was examined by taking LM PFC thicknesses of 0.1, 1.0, and 10.0 cm, followed by a thick breeding material section. This was done with one-dimensional nuclear analysis and is reported in Ref. 5. The breeding zone was a homogenized representation of the DCLL blanket for the FNSF (Ref. 70). Combinations of the LM PFC/LM breeder were examined (e.g., Sn/Sn-Li, Sn-Li/Sn-Li, and Pb/Pb-Li). Both the Li fraction in the LM alloys and the ^{6}Li fraction were varied for the breeder zone as well. The neutron multiplication properties were generally similar for Pb, Sn, and In and were much lower for other low-melting-point metals. The tritium breeding ratio (TBR) was only significantly greater than 1.0 when Pb-Li was the breeder; Sn-Li was found to be a marginal breeder, which is consistent with Ref. 71. Liquid metal PFC materials that worked best with a Pb-Li breeder were Li, Pb, Pb-Li, and Sn-Li. On the other hand, if the LM PFC is very thin, such as 1 mm thick, virtually all the LMs will perform similarly with Pb-Li as the breeder, from the nuclear point of view.

In order to understand the benefit of having a LM layer on the FW in terms of reducing the neutron damage and He production, Li, Sn, and Pb-Li were considered as LM PFCs. The thickness of the layer was varied from 0 to 30 cm, with a solid substrate assumed to be behind it. Although there were slight differences among the PFC materials, overall, about 10 cm was required to reduce the displacements per atom (dpa) by 2.5 times and about 16 cm to reduce it by 5 times. Although these results show that the nuclear damage of solids is not strongly reduced without going to thick LM layers, a 5-cm-thick

layer could reduce the peak dpa by 1.67 times, and 2.5 cm would yield a 1.25 times reduction. Since the He and H production are also neutron energy dependent, the reduction would be somewhat stronger.

Specific activities and decay heat show that Pb, Ga, and Li (assuming tritium is removed) are superior with rapid fall-off over 1 day to 1 week and continuing to 1 year. Indium starts high and only decays slowly, while Sn decays only slowly, with a little more than 10 times reduction after 1 year. The penalties of specific LM PFC materials will be dependent on volume and the potential to separate the activated impurities and transmutations from the liquid.

More detailed analysis with three-dimensional (3-D) MCNP was performed with models of a FNSF sector[5] with no penetrations. The LM thickness was fixed at 2.5 cm, based on simulations of flowing LM concepts,[8] in front of a collapsed version of the same RAFM substrate material of 34% MF82H + 67% He that made up the FW of the FNSF design, and all cases have Pb-Li as the breeder. The LMs examined were PbLi, Li, Sn, and SnLi. Lithium was taken to be 90% enriched in ^{6}Li in all cases. The presence of the LM increased the TBR in all cases above the reference by 4% to 13%, the highest being Li due to direct breeding and Sn being the lowest since it is only providing additional neutron multiplication. The neutron multiplication is enhanced with Pb-Li, Sn, and Sn-Li by up to 14%. Material damage at the substrate solid (RAFM steel) is reduced compared to the reference by the 2.5-cm LM layer between 2% to 10% on the outboard (OB) side and 9% to 15% on the inboard (IB) side. Meanwhile, He production was reduced in the range 19% to 35% on the IB side and 9% to 23% on the OB side. The strongest reductions were from Pb-Li, Sn, and Sn-Li dominantly due to neutron multiplication and lowering of neutron energies. Very similar results are seen for the H production. Overall, since the LMs of interest for the PFC application (Li, Sn, and Sn-Li) have strong nuclear reactivity, they have an important impact on tritium breeding, material damage, and He/H production that must be accounted for and are sensitive to LM layer thickness. The LM PFC concepts that have very thin layers (~1 mm) would generally have only weak impacts compared to a case with no LM PFC, and the differences between LMs would be minor. Reference 5 should be consulted for the detailed assessments.

IV. SOLID SUBSTRATES FOR LM PFCs

The LM concepts examined in this study will all have some form of a solid substrate to support the LM. This may be a FW surface, a base and mesh on the FW, a divertor flow surface, a divertor base and mesh, or tubs in the divertor, all connected to a helium cooling system similar to the breeding blanket or traditional solid divertor concepts. The interactions between the LM and the solid are clearly critical; however, the database on LM-solid interactions ranges from 30 to 60 years old and often involves materials that are not fusion relevant.[72] Recent work[73,74] shows both the importance of developing a material loss rate (kilograms per year or millimeters per year) for each LM-solid combination and carefully diagnosing the liquid-solid interlayers in order to know the long-term conditions that will develop in steady state. Pursuing RAFM alloys and their variants is important for fusion since there are no other alternative structural materials sufficiently mature to compete. On the other hand, it is well known that a number of refractory metals have good compatibility with a wide range of LMs (e.g., Mo and W) at high temperatures.[75,76] This must be balanced against avoiding high nuclear activation materials, generally restricting their use to coatings on RAFM, for example.

Reviewing the corrosion data for Li, Sn, Sn-Li, and Pb-Li, one can be seen that Li has low corrosion rates in contact with steels, and they are even lower with ferritic steels than stainless steels. The best data come from the 1980s (Refs. 77 through 83) and some earlier data summaries.[84] These experiments involved both thermal and forced convection loops. Up to temperatures of 500°C to 600°C, the thinning rate is <0.0025 to 0.025 mm/year over a wide range of flow velocities. Experiments do show higher initial material loss rates before relaxing to the slower thinning. The control of intrinsic impurities (O, N, C) in Li is critical to obtaining these low corrosion results, and the technology for this has largely been established. IFMIF represents the latest research into fast moving liquid Li; however, the effect of a magnetic field on lithium corrosion has not been established. For comparison, extensive corrosion studies have been done recently for Pb-Li since it is a primary blanket breeder candidate. Static corrosion tests for Pb-Li and RAFM steel showed ~0.04 mm/year (Refs. 85, 86, and 87), and forced convection flow at 10 to 20 cm/s showed ~0.2 mm/year (Refs. 88, 89, and 90). The forced convection in a magnetic field then resulted in ~0.3 to 0.4 mm/year (Refs. 91, 92, and 93). These thinning rates for Pb-Li are not acceptable since they could result in structural failures in too short a time frame and will require amelioration. Tin shows a more rapid corrosion rate than does Li, and in general, Sn-Li has similarly rapid corrosion. Static corrosion tests[73,94] resulted in ~3 to 15 mm/year thinning for both ferritic and austenitic steels exposed to Sn and also

showed a strong increase in corrosion rate as the temperature rises from 300°C to 700°C. The refractory metals W and Mo have good corrosion resistance to Sn even up to >900°C (Ref. 95). Whether these could be used as sustainable coatings is unclear. In contrast, the use of Al additions to steel, which forms a self-sustaining alumina layer, has been shown to be effective at reducing the corrosion in high Cr ferritic steels[96] exposed to Pb-Li, and aluminide/alumina layers show potential as well.[97] Finally, for Ga the corrosion rates[98] for steels are enormous, ranging from 30 to 50 mm/year for temperatures of 400°C to 600°C, which largely eliminates this LM as a candidate, as noted in Sec. I.

In addition, MHD in the LMs or currents intentionally driven in the LMs likely require insulating layers in order to reduce large drag and pressure drop. The use of electrically insulating materials in contact with the LM significantly reduces the pressure drop (resistance to flow) compared to conducting walls by forcing the currents generated in the conducting LM as it moves through a magnetic field to return through the fluid and produce a balanced body force over the whole cross section. These can take the form of an intrinsic layer[85] (Al_2O_3) that forms on its own an insulator coating applied on RAFM steel or a fully solid ceramic structure (e.g., SiC-SiC composite). These layers would be in close proximity to the plasma and neutron fluxes, and their sustainment and ability to provide this insulating function require verification. It should be emphasized that insulating flow paths for LMs are required anywhere the magnetic field is significant and also in the fringing field outside the main magnets (toroidal and poloidal field coils). For a FW or divertor application where high flow speeds are required, the injector apparatus would need to have insulation and might even be entirely constructed of insulating materials. The compatibility of LMs with various insulating materials is not well understood except in some particular cases (e.g., alumina and PbLi) and requires significantly more development.

A serious failure mode for LM and solid combinations is often called liquid metal embrittlement (LME) (or many other names). In this situation the LM can rapidly penetrate a solid and severely embrittle it, allowing rapid crack propagation in the solid when it is under tensile stress. Any LM-solid combination must be shown not to be susceptible to this mechanism before it can be accepted for application in a fusion reactor. This could be dependent on impurities in the LM as well as the solid. Although this mechanism has been recognized since the 1950s, it has obtained only an empirical understanding. Difficulties arise due to different mechanisms for embrittlement, different rates of embrittlement, and sensitivity to environmental conditions. There are well-known LME pairs such as Al-solid and Hg-liquid, stainless steel–solid and Zn-liquid, and steel-solid and Cu-liquid. There is a wide range of related processes including stress corrosion cracking, corrosion fatigue, and hydrogen embrittlement. There is an enormous body of literature on LME; some older references discuss observations and include Refs. 99 and 100, some attempt to coordinate observations,[101] and some recent efforts can be found in Refs. 102 and 103 although these are hardly exhaustive. Attempts to develop predictive models have generally suffered from numerous counterexamples that can be found in the experimental literature. It is critical to develop a reliable and accessible experimental process for identifying susceptibility for a given application (which would include normal and off-normal operation parameters). For example, if an accident resulted in the spilling of the LM onto the vacuum vessel (VV), the LM-VV solid combination would also require clearing against LME (in addition to the PFC substrate solid material) and at a wide range of temperatures and stresses.

V. INTEGRATION ISSUES WITH LM PFCs

The application of LMs to the plasma-facing region requires the integration of the system into the fusion plant. A simple view of this system is shown in Fig. 6, which represents the loop over which the LM is exposed to the plasma producing the hot leg, which proceeds through the tritium (and deuterium) extraction apparatus, then through a HX producing the cold leg, then through a cleanup apparatus (or multiple), and finally through an apparatus to reestablish its desired constituency (e.g., 20% Li and 80% for $Sn_{80}Li_{20}$).

The LM would begin at the constituency control where it is established to have the correct stoichiometry, ^{6}Li enrichment, and minimized impurities (irreducible impurity levels) in the cold leg. When the LM enters the plasma region, it will pick up D, T, He, Ar (radiating impurity), and corrosion products from solid substrate materials and will contain transmuted isotopes of its constituents, corrosion products, and irreducible impurities. The LM receives its heating from the plasma as surface and volumetric heat loads. After exiting the plasma region, it should first encounter the tritium (hydrogen) extraction system where the hydrogen isotopes are removed in order to keep the concentration low in the rest of the flow loop. This extraction apparatus will depend on the specific LM. The piping that provides the LM loop can introduce

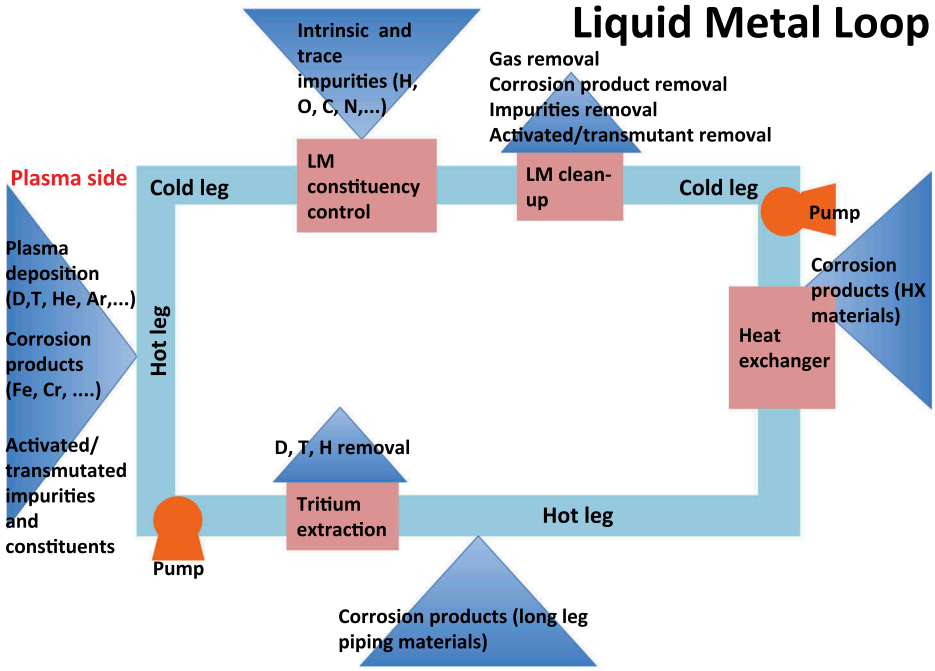

Fig. 6. A simplified LM PFC flow loop in the fusion plant.

additional impurities depending on what it is made of and the temperature and flow velocity. The LM will then reach the HX where its temperature will be reduced, and additional impurities can be introduced from the HX materials. The cold leg of the loop begins after the HX and proceeds to the cleanup systems, which is likely to be composed of a series of separate actions to remove specific types of impurities (e.g., magnetic traps and cold traps). The LM then moves to the constituency control where the main LM components are balanced, ^{6}Li is enriched to enhance breeding if necessary, and intrinsic (O, N, C) and trace impurities are introduced with the LM components. In order to model the LM loop, one requires a energy balance for the LM as a whole and a concentration balance for all constituents and impurities, presented here in a lumped parameter simplified system to demonstrate the sources and sinks:

$$\rho C_p dT/dt = \Delta \cdot (k\nabla T) + v \cdot \nabla T + S_{plas}{}^{surf} + S_{nucl}{}^{vol} - L_{heat} + h_{\mathrm{HX}}\Delta T + h_{clean}\Delta T$$

and

$$dC_i/dt = \nabla \cdot (D_I \nabla N C_i) + v \cdot \nabla C_i + S^i{}_{plas} + S^i{}_{subs} + S^i{}_{irrad} + S^i{}_{piping} + S^i{}_{\mathrm{HX}} - E^i{}_{clean} + S^i{}_{constituency},$$

where

T = bulk temperature of the LM

S = heat sources

L = heat losses

h = heat transfer coefficients

k = heat conduction coefficients

C_i = concentration of a given impurity species

S = impurity sources

E = extractions (losses)

D_i = diffusion coefficient for impurity species i.

It should be noted that although one might assume velocity profiles for simplicity, there are momentum equations that would accompany these that would provide those profiles, and more importantly, they would show flow effects that could lead to deposition or other phenomena (e.g., pipe expansions). In addition, boundary layers would be prescribed for flow velocity and mass transfer more consistently. Chemical reaction equations would also be included to account for formation of compounds and their reaction kinetics. Corrosion models[104] can be applied based on the mass loss/gain processes at work in a given region. The temperature

will dictate the precipitation of compounds formed in the LM and any chemical reactions and therefore the possibility of deposition on pipe walls or other surrounding structures. The temperature range around the loop is constrained by major requirements: Avoid excessive fluxes from the LM into the plasma region (depending on FW or divertor), and avoid all solidification or precipitation in the loop with the exception of the cleanup system, which may utilize cold trap features. In addition, there may be other impacts such as the solid-liquid material interface limits (corrosion). Because of the LM loss limits before impacting the core plasma excessively, discussed in Sec. II.A, the temperature rise from the LM inlet is restricted. This would affect the flow speed, length of the flow path, and LM thickness.

These loss limits are not known accurately, so for Li, Sn-Li, and Sn, they can be approximated by using the flux and edge plasma density correlations developed in Ref. 28, for discussion. Lithium was identified to allow a loss flux of ~2×10^{20}/m^2·s under low recycling, while Sn_{80}-Li_{20} was determined to allow a flux of ~3×10^{18}/m^2·s under high recycling. The corresponding temperature limits associated with evaporation were ~380°C for Li and ~540°C for Sn-Li. Using the fluorine result from Ref. 28 and the scaling from Sec. II.B, the tolerable flux of Sn would be ~1×10^{16}/m^2·s, with high recycling, which implies a maximum temperature based on evaporation only of about 680°C. These values ignore the ad-atom processes that might be more limiting and could be strongly affected by near-surface physics, particularly gas formation, as mentioned in Sec. II.A and discussed recently in Ref. 105.

The tritium extraction is typically done as soon as possible after the LM leaves the fusion core in order to avoid higher tritium concentrations in the rest of the loop (e.g., HX), although it could be part of the cleanup system if the LM is not being used for thermal conversion to electricity (no HX). The pipe runs throughout the loop, which would be a source for corrosion products, and should be chosen to be very similar materials to the substrates in the plasma chamber in order to avoid longitudinal (along flow path) mass transfer associated with different materials. If the LM substrate materials in the plasma chamber are made of a RAFM steel, then the pipe runs could be made of T91 (Ref. 106), which is a ferritic steel with very similar constituency but is much less expensive and is an industrially available material. If there is a HX in the LM loop, it may be more difficult to choose a material that is very similar since the HX uses optimized heat transfer metals/alloys, but interactions can be minimized. The cleanup system is critical to the viability of the LM loop and must remove a wide range of materials from the LM including gases, oxides and other compounds, intermetallics, materials in solution, and radioactive transmutations. Similarly, a wide range of approaches is used to isolate these impurities to facilitate removal, including (1) solubility/temperature dependence to create precipitation, (2) raising temperature to invoke decomposition of compounds, (3) mixing with a substance that has a higher affinity for the impurity than the LM, (4) centrifugal separation of high-mass impurities, (5) liquid-gas interface to allow the escape of gases, (6) slag skimming for cleaning off naturally separating impurities, and (7) filters to catch precipitating materials in the LM and so forth. A sequence of cleanup schemes is clearly needed and is dependent on the LM. Finally, the LM reaches the constituency control section where new LM is added and the temperature returns to its inlet value before proceeding back into the plasma chamber.

V.A. Design Windows for Plasma-Facing LMs and Thermal Conversion to Electricity

The use of liquids facing the plasma in a tokamak imposes overlapping constraints on operating parameters such as surface temperature, bulk inlet and outlet temperatures, heat flux, total power removed, flow speed, and pumping power. These are best described in the form of design windows. Temperature design windows were examined for three possible coolants (Li, Sn, and Pb-Li) in three configurations: thin flowing films, thick flowing jets, and wetted walls. Wetted walls with nearly stationary liquid films were found to behave very similarly to coated solid surfaces. Heat must conduct into an actively cooled substrate. The main concern for these designs is to maintain an acceptable surface temperature to prevent excessive contamination of the plasma, and these are being pursued.[107,108]

Flowing films are subjected to more complex constraints. The effort here focused on divertor applications, which have short exposure lengths (and times) with an expected peak local (time-averaged) heat flux in the range of 5 to 15 MW/m^2. Temperature rise and flow speed were chosen as the primary axes for representation of the windows, and parameters from FNSF (Ref. 27) were used to establish the nominal design conditions (e.g., the power levels and nominal plasma footprint).

Figure 7 shows results for 1-cm-thick flowing Li, Sn, and Pb-Li in the divertor having a 4.3-cm footprint of heat flux of 10 MW/m^2. The flow length is 1 m, the field is 7.5 T, and the slug flow is assumed with insulated

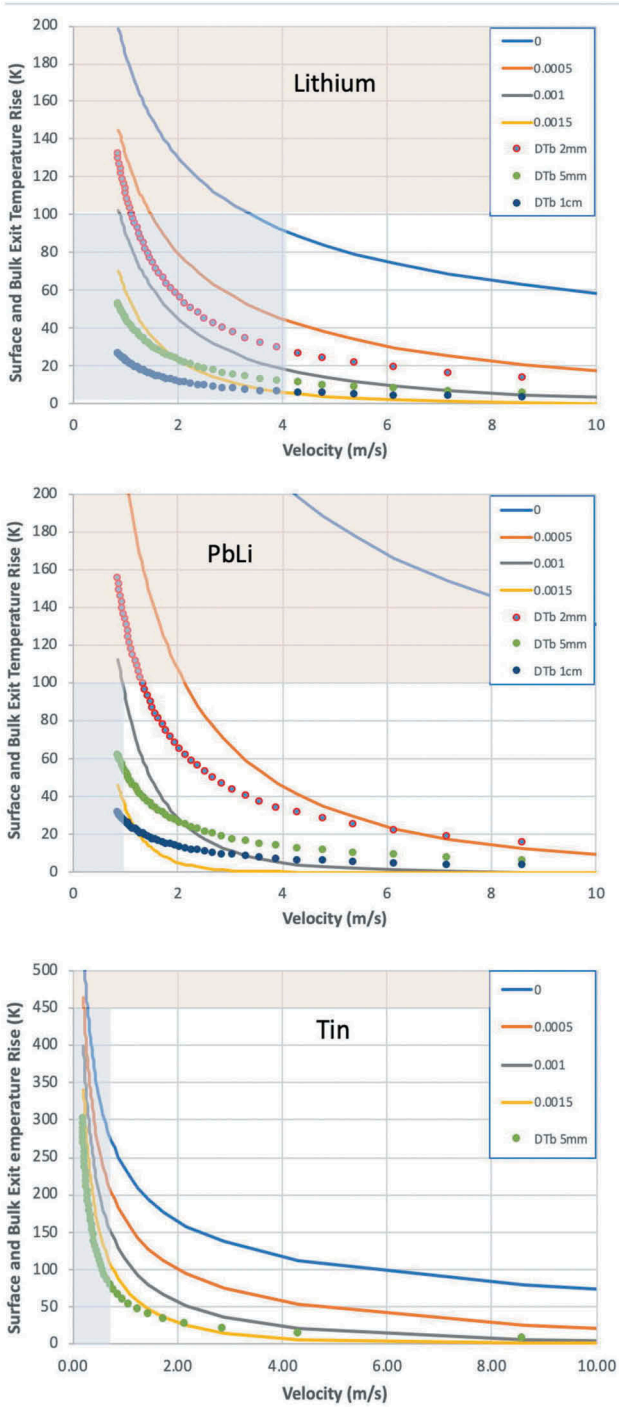

Fig. 7. Surface and bulk temperature rise of a 1-cm-thick LM film flowing over a 1-m-long divertor-like surface, subject to a localized 10 MW/m^2 surface heating. Surface (uppermost solid) and near-surface temperatures (consecutive solid curves below), and bulk temperatures through the thickness (dots).

Hartmann walls. The inlet temperatures of the LMs are all 350°C to be compatible with the lower temperature limit of RAFM steel. Figure 7 shows the exit surface temperature rise (solid and near-surface values) and exit bulk average outlet temperature rise (dotted, at three locations in the liquid layer) as a function of LM velocity. The blue box at the left is a constraint imposed by inertia and MHD body forces: Higher velocities are required in order to ensure the coolant does not stop within the 1-m length of the exposed surface. (Note that the variation in film thickness due to slowing was not considered in this simplified analysis.) The orange box at the top is a constraint imposed by evaporation into the plasma, assumed to be 450°C, 400°C, and 800°C for Li, Pb-Li, and Sn, respectively, for this examination. In all cases the bulk average temperature rise of these flowing films is extremely low. This influences the power cycle and pumping power required to maintain the flow (relative to the total power removed). Relatively high flow speed is required to maintain the surface of the lithium below the evaporation limit. Even without the inertia requirement, speeds in the range of 4 to 8 m/s are needed. Heat fluxes beyond 15 MW/m^2 will be difficult to remove. The Pb-Li case is intractable due to the low thermal conductivity (four times lower than Li and three times lower than Sn) and relatively high evaporation rate (low-temperature limit) that assumes Pb would be released. Because of its very low evaporation rate (high-temperature limit), Sn was found to have a wide operating space. Mixing of the LMs can improve these results, but previous analysis indicates that in a magnetic field, the bulk mixing of LMs can improve these projections only slightly since they result in an equivalent thermal conductivity that is only two times higher. Figure 8 shows additional cases for lithium at varied heat fluxes of 7.5 to 15 MW/m^2.

V.B. Power Conversion Impacts of Using Low-Temperature PFCs

As much as 20% to 25% of the total thermal power available for electricity generation including heating and current drive power injected into the plasma comes from surface heating. The loss of this energy would be a significant penalty due to both the lost revenue (effectively increasing the cost of electricity) and thermal waste heat load to the environment. Therefore, integration into the plant power conversion system is desirable.

In recent power plant design studies, exit temperatures from both the blanket and PFCs have been high enough to enable high conversion efficiencies (>50%) using a Brayton cycle similar to those used today in combined cycle gas turbine plants as well as next-generation fission reactor designs. The impact on

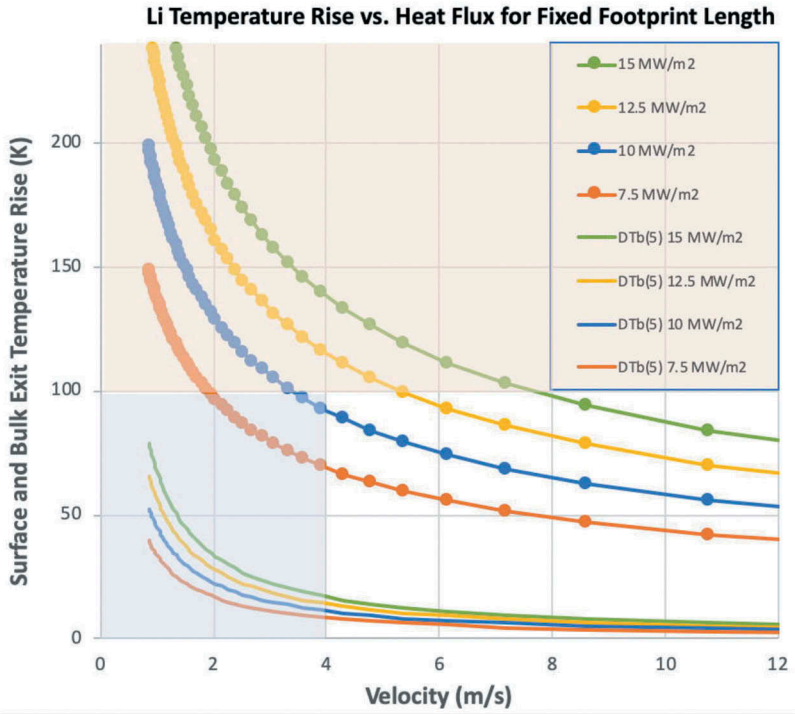

Fig. 8. Surface and bulk temperature rise of a 1-cm-thick lithium film flowing over a 1-m-long divertor-like surface, subject to a variable localized surface heating. Surface (solid with dots) and bulk temperature rise (solid), upper to lower are 15, 12.5, 10, and 7.5 MW/m^2.

conversion efficiency due to temperature constraints imposed by the use of LM divertors was evaluated quantitatively.

Two effects were considered using the ARIES-ACT1 (Ref. 109) and ARIES-ACT2 (Ref. 110) reference power plant design points: the effect of reduction in inlet temperature to the HX and the effect of reduction in the turbine inlet temperature (i.e., HX outlet). For a Brayton cycle, the inlet temperature to the HX has a significant influence on the cycle parameters and can lower the cycle efficiency if the temperature is reduced too far.

Figure 9 shows the effect of a reduction in the HX inlet temperature on the plant total electric output using ARIES-ACT2 as an example. In ARIES-ACT2, the divertor supplied the highest outlet temperature. If the He/W divertor is replaced by a liquid lithium system, then the turbine temperature will be limited by the blanket outlet temperature (620°C) instead of the higher value obtained from the He/W divertor (690°C). This was included in the results.

A loss of 125 MW would result from the use of lithium with a HX outlet temperature constraint of 300°C. For tin, almost no impact would be seen due to its high-temperature capability that nearly matches the operating temperature of ARIES-ACT2. If a liquid lithium PFC is used in the higher-performing ARIES-ACT1 power core, the total loss of gross electric power is even higher (182 MW). In this case, the loss of electric output is so large that it would be more economic to dump the heat into the environment rather than convert it to electricity.

V.C. Tritium Handling in LM PFCs

The tritium that is produced by nuclear reactions or implanted in the LM as it traverses the plasma chamber must be removed, or its concentration will build up and create permeation issues throughout the LM loop and/or inventory issues releasable in an accident scenario. This is particularly acute for Li since it efficiently breeds tritium and has a high solubility for hydrogen (even beyond solubility limits it will continue to absorb hydrogen). Tritium (hydrogen) extraction methods for LMs are in a low state of development although concepts have been studied, and in some cases, small demonstrations have been accomplished.[111] Some techniques for Li include the Maroni process (contact with molten salt), electrolysis, and evaporation/distillation. For most other LMs (with much lower affinity for hydrogen) and even He coolant, the permeator window is considered a primary candidate.

Figure 10 shows a simple tritium flow loop diagram, highlighting the plasma fueling/exhaust and blanket

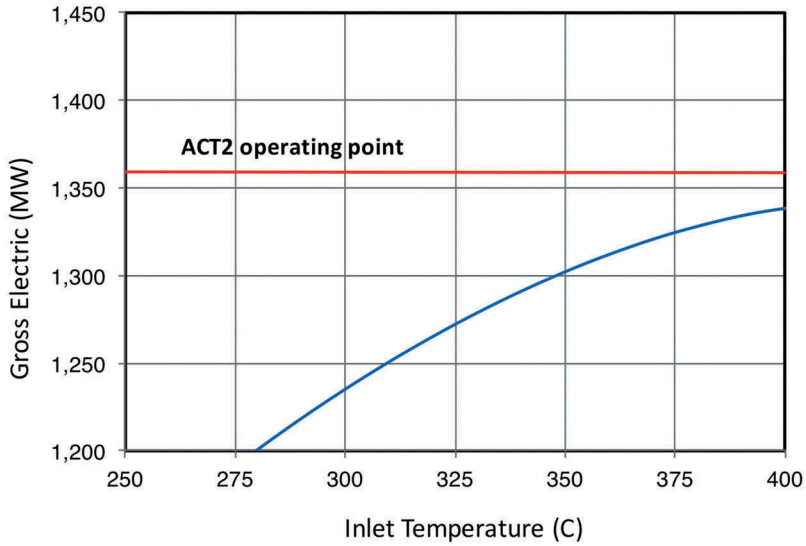

Fig. 9. Gross electric power produced by ARIES-ACT2 as a function of HX inlet temperature (horizontal line is baseline value). The turbine inlet temperature also was reduced due to the elimination of high-temperature helium from the divertor (which had produced the highest system temperature in ARIES-ACT2).

breeding loops. The LM PFC introduces a new fluid to the original system in the FNSF, which originally contained the blanket He coolant, the divertor He coolant, and the blanket breeder LM (Pb-Li). Each of these fluid streams requires its own tritium extraction, HX, and cleanup system based on what the fluid is and also the operating temperature of the fluid.

Attempts to make the PFC and blanket breeder LMs the same material have been difficult. Sn-Li is a poor breeder material, and Pb-Li is unattractive as a PFC material due to the large Z of Pb and higher evaporative losses compared to Sn or Sn-Li. Using Li as the blanket breeder would increase the inventory of Li significantly beyond what is necessary for a PFC application, and the reactivity of Li and its safety implications have largely eliminated it from any blanket concepts being considered at present. IFMIF is the only large-scale application of liquid Li, with significant development and prototyping.

V.D. Helium Pumping from the Plasma Chamber

Helium pumping with LM PFC systems is generally considered necessary since it does not chemically bond to any of the LMs nor is it soluble in any of them. This pumping requirement would extend to other gases like argon or neon that might be injected to enhance radiation from the core plasma. Analysis in Ref. 112 implies that to remove appropriate levels of He to control the core content, the He diffusion coefficient needs to be $<10^{-8}$ m^2/s to allow reasonable flow speeds of the LM (tens of meters per second) for 10-keV incident He ions. Lower He energies would have a too-shallow depth of deposition, faster diffusion coefficients would allow the He to reach the surface quickly, and a too-slow LM flow would also allow the He to reach the surface before it left the plasma chamber. Ref. 113 subsequently identifies the He diffusion coefficient in flowing Li to be 2.5 to 6.5×10^{-7} m^2/s, which would require >100 m/s flow velocity for the highest He energies or even higher speeds for lower He energies. Although bubble formation or He concentration near the LM surface might lead to a more tenable solution, overall, it does not appear that He can be removed by any LM PFC candidate sufficiently well to rely on it to keep the core plasma from diluting, thus requiring pumping of gaseous He. This creates the undesirable feature of also pumping Li vapor for a Li PFC or smaller amounts of other LM PFC candidates into the plasma exhaust system simultaneously with the He. Some technique for depositing the Li or other LM while letting the He pass through will be required.

V.E. First-Wall Penetrations

The FW and blanket are penetrated by several systems that support the plasma operation, primary of which are the heating and current drive and the diagnostics. The FNSF physics assessment[114] identified ~8 m^2 for neutral beam (NB), LH, IC, and EC heating and current drive access and ~3 m^2 for diagnostics access. If a flowing LM PFC system is being applied to the FW, then it must have

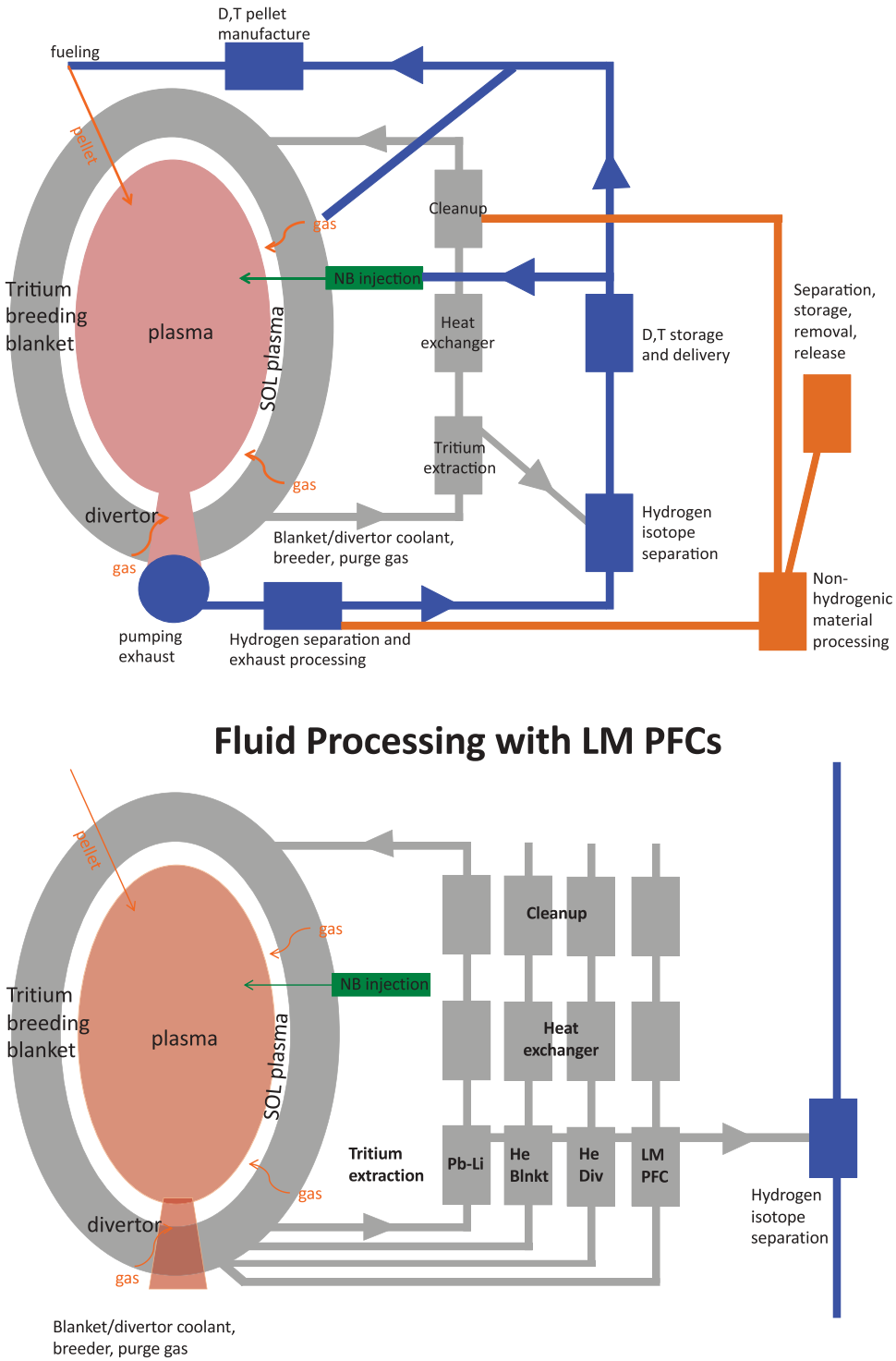

Fig. 10. Simplified plant tritium flow loops and expansion of the blanket, divertor, and PFC fluid loops showing the need for individual processing for each fluid or operating condition (e.g., temperature).

a way of bypassing the penetration. Specific geometries are likely to be required to minimize disturbing the flow while diverting it around the hole. For some sources (NB) the hole size is a large fraction of a sector area, and different injection approaches might be required. This sort of design and optimization can be addressed in a flowing LM experiment and requires 3-D MHD LM simulations. On the other hand, a capillary system composed of smaller blocks or tailored shapes may have an easier time in accommodating penetrations on the FW.

The presence of a hole on the FW, regardless of what is in it, will allow the possibility of LM vapor depositing on the exposed equipment (e.g., straps in an IC resonance frequency launcher, waveguides in a LH launcher). The condensation of the LM vapor on surfaces or having vapor in the region can disrupt operation or degrade performance. Depending on the LM, it may be chemically reactive like Li and form compounds on the structure surfaces. Operating the launching structures at high temperature, which is likely, is a common approach to avoid deposition, although it may increase the power losses in the launcher itself.

V.F. Pumping LMs

The LM PFC concepts that introduce the LM into the plasma chamber by injection or capillary forces will lose control over the fluid flow. The fluid must be collected and drained out of the plasma chamber largely by gravity and any initial injection force that persists. It has been found in IFMIF prototypes[115] that the LM must be collected into an accumulation tank, and sufficient elevation must be maintained before it can be pumped on or cavitation will result, and this is now part of the Li systems in the fusion neutron source. This is most easy to visualize for flowing systems. In capillary systems the LM may be allowed to evaporate, or it might be collected and recycled as part of the design. Since the LM adheres to the roughened surface or mesh on the substrate, it will only move if it is overfilled above the height of the irregularity, and the speed of flow would depend on this excess height.

V.G. Magnetic Fields and LM Flow Geometry

Figure 11 shows the basic picture of LM flow over the FW, which is launched from the top of the device and flows down the walls to the divertor at the bottom of the device, under the influence of gravity and centrifugal (produced by the injection of the LM) forces. In the divertor the LM can land in a tub (full of LM), or it can continue on specifically designed surfaces to guide it to the drain where it leaves the plasma chamber. Focusing on the FW, the geometries of the IB and OB surfaces show there is an outward toroidal curvature and an inward toroidal curvature, respectively. There is poloidal curvature only on the OB surface. Otherwise, the width of a flow path on the IB is constant, while on the OB it is narrow, expands, and then narrows again, leading to flow speed and thickness variations. A detailed examination

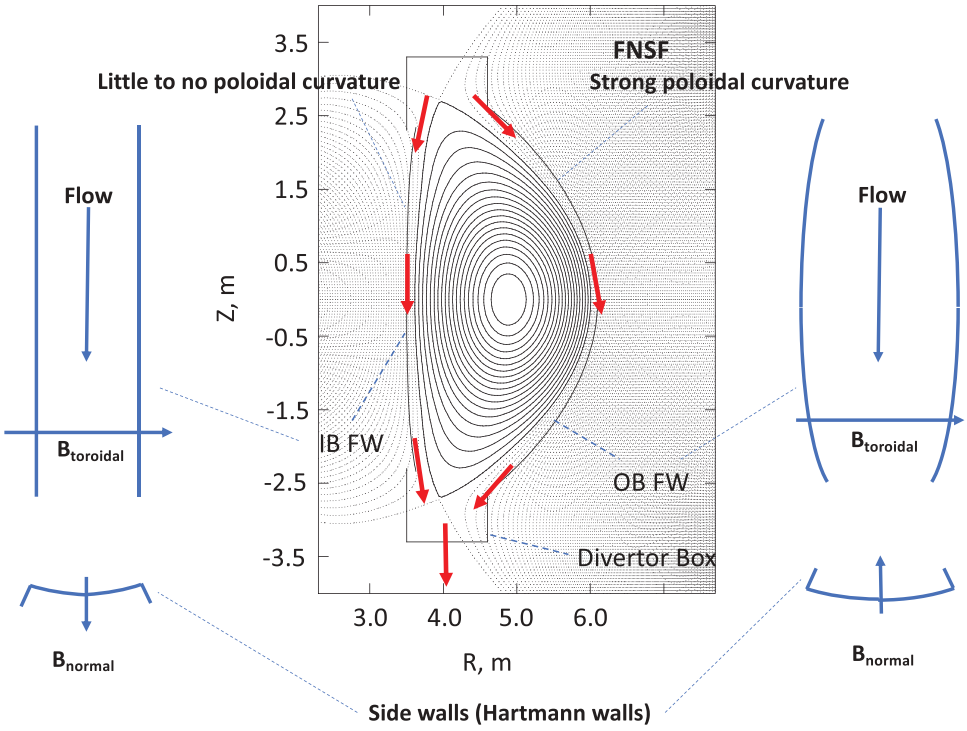

Fig. 11. The plasma cross section with FWs on the IB and OB sides. The divertor boxes are also shown. The IB and OB flow path geometries are also shown, giving the curvatures. Side walls are shown for the flow path, which may or may not be present.

shows the FNSF equilibrium magnetic fields on the IB, which the conducting LM must flow through. They range from 9.8 to 10.3 T (toroidal field) and 0.0 to 0.06 T (normal field, poloidal field) on the IB side, and 5.9 to 8.0 T (toroidal field) and 0.0 to 0.15 T (normal field, poloidal field) on the OB side. These include the plasma and can have up-down asymmetries in the normal field of about ~0.01 T due to plasma position. The primary magnetic field is the toroidal field, which is perpendicular to the flow and simultaneously is perpendicular to the side walls (called Hartmann walls). This is the field largely responsible for large drag on the fluid and the associated pressure drop. The normal field, which is normal to the surface on which the free-surface LM is flowing, is much smaller but has a significant effect on the flow.[8] The maximum toroidal field ripple is ~0.0016 T, and the nonaxisymmetric field is estimated to be ~0.0003 T, both considered too small to affect the LM MHD.

Simulations of the flow with MHD fluid and thermal analysis[8] show that the fluid thickness, flow length, velocity, and heat flux all play a role in the design of a flowing system. Here, for the FW the heat flux was low, ~0.2 MW/m^2, to represent the radiative heat flux from the plasma only. The LM, Li in this case, was examined with an entrance temperature of 350°C to observe the lower temperature limit of the RAFM steel substrate. The flow lengths were ~5 to 10 m in length. Velocities ranging from 1 to 20 m/s and initial thicknesses of 0.005 to 0.08 m were examined. In general, the temperature rise was only 30°C to 40°C, allowing Li to stay within its maximum tolerable loss rate (less than ~380°C). In addition, the temperature rise was restricted to the outer half of the fluid thickness, only barely affecting the substrate if at all. Clearly, higher heat fluxes would require higher velocities. Initially, the analysis assumed that the FW would be toroidally continuous, with no divisions. Under these conditions for the IB FW, with a toroidal field of 10 T and a normal field of 0.05 T, the optimum combination was an initial fluid thickness of 0.02 m and an injection velocity of 1.7 m/s, giving a uniform thickness throughout the flow length. This resulted in an allowed temperature rise. Maintaining uniform LM thickness is critical to avoid plasma contact or interference with SOL flows. In particular, height changes could allow the LM to receive a much higher heat flux by changing its geometry relative to the magnetic field lines, which carry the particles and energy.

On the OB the situation is more complex with the strong poloidal curvature and requires higher flow velocities to create a centrifugal force that pushes the LM against the FW surface. Similar temperature rises, keeping Li within allowable losses, can be achieved with velocities of 2 to 10 m/s; however, maintaining a fixed LM height is challenging with the presence of more substantial normal fields of 0.03 to 0.06 T in these simulations with both varying flow velocity and normal field value. The toroidally continuous case had LM height variations of two to three times the initial injected height in the course of the flow down the FW. The introduction of dividing walls on a sector allowed solutions with significantly weaker thickness variations. This was consistent with maintaining the tokamak since it is necessary to segment the fusion core for removal, and side walls along the edge of the sector could be incorporated. It is important to recognize that the side walls are considered to be electrically insulated, which may be difficult in the FW location. A comparison of the toroidally continuous and divided wall cases with initial LM height of 0.02 m, and 5 and 10 m/s flow speed, for the IB and OB can be seen in Ref. 8.

VI. TECHNICAL INVESTIGATIONS IN LM PFCS

A series of technical investigations was made into areas relevant to assessing the viability of LM PFCs, noted in Sec. I, and some of these are summarized here.

VI.A. Tritium Behavior and Accident Scenarios

Various tritium transport scenarios in the FNSF using the MELCOR/TMAP model have been examined.[4] These include the original design with a solid FW and variations with LM PFCs of Li, Sn, and SnLi. The liquid wall model assumes a 1-cm-thick FW layer flowing at 10 m/s into a tublike divertor.

In the solid-wall design, tritium losses from normal operations were similar to our original TMAP model ~23 g/year for 80% efficient extraction from PbLi and ~10 g/year for 90% efficient extraction from PbLi (Ref. 116). This is dominated by losses from the pipes in the PbLi cooling system. In all of the LM wall cases, we found that transport of implanted tritium in the FW and its associated loop was essentially decoupled from transport of bred tritium in the blanket and its associated loops, i.e., the losses from the blanket, structural ring, VV, and associated piping were essentially unchanged by the presence of the LM FW and divertor.

Additional losses from the FW LM loop piping depend on assumptions about the size of this system as well as the kinetics of implantation and desorption at the

plasma-LM interface. For Sn and SnLi, which have low hydrogen solubilities, we have assumed that the desorption process is fast relative to convective transport along the wall[112] and simply scaled the implantation flux by measured retention fractions (~2E–4) for Sn and SnLi exposed to a deuterium plasma.[35] Provided this assumption is valid, losses from the FW loop piping are comparatively small, ~0.01 g/year. For lithium, we assume 100% retention of impinging hydrogen. In this case, it is the inventory in this loop we are concerned about, assuming it may be released during a fire or other accident. If the extraction system is 70% efficient (single pass) and this system can be located within 10 m of the vessel inlet/outlet, inventories are kept to ~3 g, which is an order of magnitude or so lower than the amount that would result in a dose of 10 mSv to the maximally exposed individual, the limit imposed by the U.S. Department of Energy (DOE) Fusion Safety Standard (DOE-STD-6003-96). Work continues to examine what other consequences a fire of this nature would have, i.e., on heat removal in accidents.

VI.B. Edge Plasma Modeling for Liquid Lithium Walls

Edge plasma modeling is used to predict the interface behavior between the deuterium-tritium (D-T) ions making up the core particle exhaust and the lithium vapor evaporating from the liquid walls.[2] Because the evaporation depends strongly on the surface temperature, the largest lithium source is expected near the divertor plates. A set of steady-state edge plasma solutions is found where upstream, adjacent to the core plasma, the D-T ions dominate, while in the divertor region, lithium ions dominate, having densities in excess of 10^{21} m^3. The high lithium density results in strong lithium line radiation that dissipates more that 90% of the exhaust power and results in peak wall power loading of ~2 MW/m^2 in the divertor region. The lithium flux from the divertor plate and nearby walls needed to reach these conditions corresponds to evaporation fluxes at surface temperatures in the range of 700°C to 750°C. A key question is the density of lithium ions reaching into the pedestal region a few centimeters inside the magnetic separatrix, which is found to be in the range of 10% to 20%, implying significant D-T fuel dilution in the fusing core. The core lithium level is controlled by the ion and electron thermal force effect along the confining magnetic field lines. The precise value of the ion thermal force is uncertain in these high-density cases, while the electron thermal force values are better understood; removing the ion thermal force effect results in a factor of ~2 reduction in the core lithium level. The core lithium level roughly scales as $P_{SOL}/(n_{core})$ (Ref. 2), where P_{SOL} is the power flux into the SOL and n_{core} is the D-T density in the edge of the core region. The power scaling can be affected by introducing a moderate-Z impurity such as neon or argon to radiate some of the core power in the edge region, but limited studies with neon show a modest effect; argon should be analyzed in future work. While the base cases assume that D-T ions and atoms are fully pumped when they flow to the lithium surfaces, lithium-hydride formation is known to be temperature dependent. But, even if the hydride formation is limited (small pumping), the basic properties of the radiative solutions remain largely unchanged. Simulations show only small differences in the lithium solutions for D-T pumping in the range of 5% to 100% and may extend to even smaller pumping rates. The D-T particle fluxes to the lithium walls are concentrated in the divertor region, but their magnitude is controlled by the total D-T particle flux across the separatrix. Base cases have peak D-T wall fluxes of ~2×10^{21} particles/(m^2·s) when the total D-T throughput is ~1×10^{23} particles/s. This wall flux is quite insensitive to the assumed D-T ion/atom pumping rates because such changes primarily affect the D-T ion and atom divertor densities rather than the wall fluxes.

VI.C. Liquid Metal Experiments

The Center for Plasma Material Interactions (CPMI) at the University of Illinois specializes in understanding the science behind plasma-material interactions and development of technologies behind PFCs. In particular, CPMI has a focus on developing and understanding liquid lithium and other LM technologies in the context of how they can be best used in fusion devices. The latest results from CPMI's toroidal fusion device Hybrid Illinois Device for Research and Applications (HIDRA) and the latest results on lithium-metal infused trenches (LiMITs) are reported.[7] A full-size LiMIT limiter plate is being built and will be tested in CPMI's toroidal fusion device HIDRA. Concurrently, an all high-Z flowing liquid lithium (FLiLi) limiter plate fabricated by Princeton Plasma Physics Laboratory (PPPL) will also be tested in HIDRA. LiMIT and FLiLi are two concepts to flow lithium down the front face; because of HIDRA's fivefold symmetry, a direct comparison between the two plates can be performed. Different aspects of these technologies will be tested for reliability before or in parallel with full deployment in EAST. A new version of LiMIT is being developed using a mesh of refractory metals to test out new ideas in using thermoelectric MHD drive to flow

LMs. Finally, results from the first active lithium hydrogen/deuterium (LiHD) distillation system will be explored. LiHD will eventually be part of a fully integrated liquid lithium loop system being proposed at CPMI to study not only the recycling effects of lithium but also the absorption rates and the technology needed to retrieve hydrogenic species (e.g., deuterium and tritium, which are reactor fuel) and reuse back in the device.

VI.D. Flowing LM PFC Simulations and Design Exploration

Utilizing an already established fusion design, the Fusion Energy System Studies group used FNSF to explore free-surface LM flows[8] to establish critical design parameters. The reference design is a tokamak-based machine with 518 MW fusion power, 4.8-m major radius, 1.2-m minor radius, and machine average neutron wall loading of ~1 MW/m^2. For this design, a PFC concept that implements a flowing LM FW and an open-surface divertor is developed. The flowing LM first removes the surface heat flux from the FW and then proceeds to the lower section of the vacuum chamber to form a large LM surface for absorbing high-peak surface heat flux in the divertor region. In pursuing the application of large open LM surfaces in the FNSF, two new computer codes have been developed and then applied to the analysis of free-surface MHD flows and heat transfer, including fast thin flowing liquid layers over the solid FW (liquid wall), a tublike divertor, and a fast flow divertor. The analysis is aimed at optimization of the liquid wall design by matching certain proposed design criteria and also an evaluation of the maximum heat fluxes, using liquid lithium (Li) as a working fluid. It was demonstrated that the flowing Li FW can tolerate a surface heat flux up to 1 MW/m^2, while the open-surface Li divertor can remove a maximum peak heat flux of 10 MW/m^2.

VII. LIQUID METAL PFC CONCEPTS AND THE RESEARCH FOR LM PFCs

The LM PFC concepts themselves provide a valuable organizing principle for R&D in this area since many viability aspects are tied to the geometry, environment, and operation characteristics. Recent concepts under consideration include (1) flowing LMs over a surface (FW or divertor),[8] (2) capillary systems distributed over a surface (FW or divertor),[107,108,117–119] (3) lithium gas/vapor box divertors,[44–46] (4) tublike divertors,[8,120] and (5) LM jets in the divertor.[121–124] These will not be reviewed in this paper, but particular aspects will be identified when exploring experimental facilities and capabilities.

A series of parameters can be developed that describe a concept's operation and environment in which the LM PFC must exist. Here, we are using the FNSF configuration and establishing a LM PFC option in an otherwise conventional fusion device design. These directly inform the attributes and upgrade path of the experimental apparatus to more prototypical parameters that are required to study the LM PFC system. Some of these are listed as follows:

1. B-field magnitude and variations
2. LM flow speeds
3. LM injection and recovery schemes
4. temperatures
5. LM thickness
6. plasma heat flux and its distribution
7. plasma particle flux and energy distribution
8. LM constituency, base and impurities
9. geometry of flow path
10. LM fluid MHD effects
11. substrate materials and their impurities
12. substrate material geometry (e.g., roughening)
13. steady and transient loads (heat, particles).

For example, flowing LM systems are most easily accessed with chute experiments,[125,126] where a wide range of LM phenomena can be explored. Clearly, the chute (length, width, and materials) must be designed to access behavior of interest for the operating parameters. Liquid metal MHD behavior can be studied with any LM, such as Galinstan due to its ease of use, while LM specific areas such as corrosion or losses require the actual LM of interest. Flow geometries (horizontal, vertical, curved, cross-section changes) should be prototyped. Moving toward more prototypical parameters (typical of a fusion device) such as temperatures would ultimately require a vacuum enclosure. Simulating the magnetic field is critical for systems with flow that induce MHD effects and include all components (toroidal field, normal field, and field gradients) that can impact the flow. It is difficult to achieve the magnetic field strength anticipated in a fusion device in one of these experiments, and dimensionless parameters can be used to clarify physics regimes accessible. Although LM safety aspects are always important, safety becomes a critical issue with increasing performance levels in the

LM experiment (higher temperature, flow speeds, LM reactivity, high pressure/pumping). Simulation of the plasma exposure, which includes vacuum, heat flux, and particle flux, may be difficult to integrate in an off-line experiment. Plasma confinement devices (e.g., tokamaks and stellarators) provide useful platforms with self-consistent magnetic fields, particle energy distributions, and geometry but suffer from low duty cycles and difficulty in diagnosing phenomena of interest. Linear plasma devices are somewhat less self-consistent in their environment (in representing the actual fusion device) but have much higher duty cycle and generally good diagnostic access. Heat (lamps) and plasma particle sources (plasma gun) can be used with off-line experiments to approximate the plasma environment but might have limited coverage on the LM compared to full extend of the LM flow, for example.

Considering a capillary porous system based on blocks,[108] a very similar apparatus can be envisioned for testing, albeit where flow is less critical, although flow induced by overfilling might be of interest as well as recovery of LM if complete evaporation is not practical. The block should have various orientations, and a wide range of capillary designs (plasma-facing geometry, pore supply geometry, reservoir, substrate materials) would be tested. With the minimization of LM flow aspects, the emphasis shifts to the plasma exposure, capillary fluid dynamics, solid substrate engineering, and large capillary structure versus alignment of many small capillary blocks. With the thin layers typical of capillary concepts, the solid substrate strongly participates in power handling.

Recalling the multiple LM properties of interest and integration needs, these can inform the experiments to be done on the apparatus as well as simulation activities to pursue to develop predictive capability, for example,

1. identifying loss mechanisms from the LM, vacuum interface and plasma
2. LM segregation of LM alloys, its sustainment in flowing LM and low flow regimes
3. wetting of LM to substrate materials, full flow regime
4. impurities in the LM, impacts and control
5. hydrogen uptake and removal (hydriding)
6. corrosion of substrate materials by the LM
7. core plasma impact of a LM
8. nuclear properties of LM and modifications to its unirradiated behavior
9. LM properties (solubilities, thermal conductivity, etc.)
10. flow obstructions, FW penetrations
11. flow over different substrates, conducting and nonconducting
12. impact of B-field gradients and small normal fields on flow
13. injection nozzle optimization
14. LM loop and its various apparatuses
15. heating, mixing, turbulence.

Depending on the LM PFC concept and the critical behavior to explore, these examinations can require a range of platforms including

1. single- to few-effect apparatus (e.g., heat flux, hydrogen uptake)
2. plasma/vacuum via confinement device, linear plasma device, or similar
3. loop simulator to explore the hydrogen extraction, LM cleanup, HX, and corrosion
4. off-line flowing/capillary/tub/jet concept experiment (e.g., chute in the case of flowing LM systems)
5. neutron exposure.

These can be encapsulated into a research strategy that has the following steps:

1. Establish a model design for a specific concept for a fusion nuclear application (DEMO, FNSF, or other), which forces the determination of many critical parameters (and assumptions) and operational characteristics of the LM PFC.

2. Examine at least the three primary candidates for LM PFCs, Li, Sn-Li, and Sn since there is insufficient evidence to eliminate any of these at present.

3. Use the characteristics of the concept to establish a basic prototypical experimental apparatus that allows access to the behaviors expected in a fusion device (e.g., chute for flowing LMs).

4. Establish other apparatus to obtain physics that is difficult or impossible to access on the prototypical apparatus (e.g., corrosion tests, tritium extraction).

5. Establish approaches to obtain plasma exposure, via confinement devices, linear plasma devices, or other, preferably well diagnosed and informative on critical issues for the concept and the complex plasma-LM interactions overall.

6. Develop simulations in parallel to any experimental activities to accelerate the development and interpretation of experimental results and improve projections to the fusion operating regime.

VIII. DISCUSSION AND CONCLUSIONS

The use of LMs as PFCs has potential benefits that can easily be understood to alleviate issues with solid PFCs in the fusion plasma environment. These include the elimination or mitigation of surface heat flux; plasma particle erosion and reconstitution; nuclear damage and transmutation; and strong gradients in temperature, heating, damage, and transmutation. Going beyond these conceptual benefits, it is necessary to explore the practical application of these systems. The LM PFC candidates, Li, SnLi, and Sn, have been explored, along with Pb-Li due to its importance for blanket breeding, to identify critical aspects requiring research that can contribute to a strong technical basis for LM PFCs. Of the low-melting-temperature elements with low evaporation rates over 300°C to 800°C, Li, Sn-Li, Sn, Ga, Ga-Li, In, In-Li, and Pb-Li were identified. However, Ga and In have resource complications, and Ga has aggressive corrosion of steels, so they were eliminated.

Liquid metals in the plasma chamber are subject to losses (ultimately entering the plasma), which strongly limit their operating temperature, composed of sputtering, ad-atom, and evaporation. More precise prescriptions are required primarily for the ad-atom component, and lower-energy range data are required for sputtering and self-consistent physics treatments of the complex interface of LM surface, sheath, vapor, and plasma environment.

A tolerable plasma content of the LM candidates can be established that does not compromise the fusion power (or neutron wall load), the divertor heating, and current drive efficiency and are tied back to the maximum allowed losses from the PFCs.

In the case of LM alloys, such as Sn-Li, the possibility of surface tension–induced segregation of Li to the surface may provide some beneficial properties compared to Sn or Li alone. This area requires more research to establish whether it can be created and sustained in a prototypical LM PFC situation.

The wetting of LMs to their solid substrates is absolutely essential to capillary PFC concepts; however, their importance to large-scale fast flowing LMs is less clear. The behavior of wetting is dependent on the LM and substrate, their impurities, time, and temperature, indicating that prototypical conditions of a LM PFC are needed to properly understand its effects in a fusion device.

Hydrogen uptake and retention are important due to the presence of large quantities of deuterium and tritium in contact with the PFCs in the plasma chamber. Although Sn and Sn-Li appear to behave like solid metal PFCs with low retention, Li has been observed to have high uptake and retention. The possibility of hydriding (formation of LiH as a solid in Li solution) is a serious concern for Li and requires further investigation, and it is expected to depend on the LM PFC concept, with very thin LM layer and slow-moving concepts the most susceptible. The hydrogen uptake behavior has considerable contradictory results in the literature due to the wide range of approaches to approximate the fusion environment (e.g., temperature, gas or plasma, stationary or moving) and requires more detailed investigation.

It is important for the LM PFC community to begin characterizing the LM composition, particularly the impurities in these LMs, on a routine basis. Historically, LM impurities have been found to impact basic LM properties as well as their interactions with solid substrates. This includes surface contamination in a wide range of experiments with free-surface LMs. In addition, corrosion products from the substrate materials and other materials in the LM loop will also be present in the LM, and all impurities will be exposed to neutrons in the plasma chamber. A significant effort is required to understand and control the constituency of the LM by identifying impurity sources and establishing the required cleanup technologies.

A unique exploration of the nuclear impact of LM PFCs shows that since the LMs of interest for the PFC application (Li, Sn, and SnLi) have strong nuclear reactivity, they can have benefits on tritium breeding, material damage, and He/H production when the LM layer thickness is >2 cm. Liquid metal PFC concepts that have very thin layers (~1 mm) would generally have only a weak impact compared to a case with no LM PFC, and the differences between LMs would be minor.

For the LM concepts considered in this study, a solid substrate is required. Because of the proximity of the substrate to the plasma, it must be a fusion-relevant structural material, such as RAFM steel or one of its more

advanced variants. Corrosion of the substrate by the LM is the major issue, although the substrate does constrain the LM operating temperature. Lithium demonstrates weak corrosion of steels in flowing tests, although data on corrosion in a magnetic field are missing. Because of its popularity as the blanket breeder material, Pb-Li has received considerable attention in the corrosion area. For comparison, it reaches thinning of 0.04 mm/year for static tests, ~0.2 mm/year for flowing tests, and 0.3 to 0.4 mm/year for flow in a B-field. This situation will require some form of amelioration. Tin shows strong corrosion thinning of about ~3 to 15 mm/year for steels, which is clearly unacceptable, and amelioration is required. Insulation of flow channel walls is generally required for LM flows in order to reduce the pressure drop (drag), and free-surface flows also benefit from this, particularly since many LM PFC concepts have high flow speeds. The data on interaction of LMs with insulator materials are very sparse and must improve considerably. Insulating materials are needed both near the plasma where the LM is a PFC but also in feed lines and injectors used to bring the LM from outside the fusion core into the plasma chamber.

The effect often referred to as LME is a real showstopper for any LM-solid substrate combination that shows this behavior. The LM penetrates the solid through grain boundaries, cracks, or defects and causes rapid embrittlement and crack propagation when the solid is in tension. Regardless of whether the crack propagation takes milliseconds or months, it is unacceptable in a fusion power system. All LM-solid combinations that exist in the fusion facility under normal or accident conditions must be cleared for this phenomena. Of the LM candidates considered here, only Li has been identified as an LME pair with some specific steels that are not considered fusion relevant. Unfortunately, the understanding of LME is still incomplete and empirical.

Any LM PFC will actually be a LM loop that recirculates the LM and contains as major components the plasma chamber, tritium extraction, HX, cleanup systems, and constituency control. Around this loop the LM would have varying temperature, major and impurity constituents, and flow speeds. The sources and sinks for these would be distributed around the loop. Understanding the loop behaviors is critical to establishing the credibility of a LM, for example, the tritium content or the activated constituent inventories and the potential for deposition of LM components within the loop.

One potential advantage of LM PFCs is to remove the surface heat flux that would normally be incident on a solid PFC surface. In a fusion power plant this can be about 20% of the available thermal power that is converted to make electricity. Because of the temperature limitation of LMs, to avoid excess losses, and the requirement that LM inlet temperatures must not be below 350°C for the RAFM steel substrates, the design windows for LM PFCs can be quite limited. There are other possible temperature limitations such as corrosion as well. It is not clear that any of the LM candidates can be effectively used in the thermal conversion cycle; even Sn may be severely constrained by its corrosion behavior.

Tritium handling is a major technical aspect of any fusion device, and in the particular case of Li as a LM PFC, it takes on a different nature. Since the Li is introduced into the plasma chamber and has contact with the D and T fueling, as well as tritium bred in the Li itself, it can contain a very large tritium inventory compared to what is typically in a LM breeder loop, for example. Since the burnup of tritium (and deuterium) fuel is expected to be low, a large amount of excess tritium is injected and exhausted from the plasma chamber, ranging from 10 to 100 times the amount that is consumed. With a Li PFC all this tritium could end up in the Li because of its strong hydrogen uptake although some may be pumped out with He and other noncondensables. In a device with solid PFCs or a LM PFC with low hydrogen uptake and retention, this fueling inventory would be in a gaseous loop exhausted from the plasma chamber with a vacuum pump. Lithium's high solubility for hydrogen can be viewed as an advantage in reducing permeation; however, in an accident scenario the Li could release the tritium in a fire. An examination of this can be found in Ref. 4.

Other integration aspects include He pumping, which is required to avoid buildup in the plasma core; accommodating penetrations for plasma heating and current drive; pumping LMs into the plasma chamber and getting them back out; and detailed descriptions of the magnetic fields and flow geometries in assessing LM PFCs.

The R&D required to establish a credible database for LM PFCs involves addressing several issues associated with the LMs themselves, their interactions with solid substrate materials, integration of LM PFCs into the fusion plant, and the various physics of the individual concepts themselves. Continued activities in the design of LM PFCs for a fusion device provide a much-needed focus for R&D toward prototypical parameters and environments. The complexity of LM behaviors requires a simultaneous and dedicated simulation development thrust appropriately validated with experiments.

Acknowledgments

This material is based upon work supported by the DOE, Office of Science, Office of Fusion Energy Sciences, under contracts DE-AC02-76CH03073 (Princeton Plasma Physics Laboratory), DE-AC 09-08SR22470 (Savannah River National Laboratory), DE-AC52-06NA25396 (Los Alamos National Laboratory), DE-AC52-07NA27344 (Lawrence Livermore National Laboratory), DE-AC 05-00OR22725 (Oak Ridge National Laboratory), and DE-AC07-05ID14517 (Idaho National Laboratory).

ORCID

C. E. Kessel http://orcid.org/0000-0002-2072-1134
P. W. Humrickhouse http://orcid.org/0000-0003-1641-5457
Y. Katoh http://orcid.org/0000-0001-9494-5862
A. Khodak http://orcid.org/0000-0002-8273-6614
B. Pint http://orcid.org/0000-0002-9165-3335
S.-J. Yoon http://orcid.org/0000-0003-0012-7805

References

1. C. E. KESSEL et al., "Overview of the Fusion Nuclear Science Facility, a Credible Break-In Step on the Path to Fusion Energy," *Fusion Eng. Des.*, **135**, 236 (2018); https://doi.org/10.1016/j.fusengdes.2017.05.081.
2. M. E. RENSINK, T. D. ROGNLIEN, and C. E. KESSEL, "Modeling the Edge-Plasma Interface for Liquid-Metal Walls in FSNF," presented at 23rd Topl. Mtg. Technology of Fusion Energy (TOFE 2018), Orlando, Florida, November 11–15, 2018.
3. A. KHODAK, C. KESSEL, and M. TILLACK, "Design and Analysis of the Liquid Metal Free-Surface Divertor Cooling System," presented at 23rd Topl. Mtg. Technology of Fusion Energy (TOFE 2018), Orlando, Florida, November 11–15, 2018.
4. P. W. HUMRICKHOUSE, S.-J. YOON, and B. J. MERRILL, "The Impacts of Liquid Metal Plasma Facing Components on Fusion Reactor Safety and Tritium Management," presented at 23rd Topl. Mtg. Technology of Fusion Energy (TOFE 2018), Orlando, Florida, November 11–15, 2018.
5. T. D. BOHM et al., "Initial Neutronics Investigation of a Liquid-Metal Plasma-Facing Fusion Nuclear Science Facility," *Fusion Sci. Technol.*, **75**, 429 (2019); https://doi.org/10.1080/15361055.2019.1600930
6. J. BLANCHARD and C. MARTIN, "Thermal and Electromagnetic Transients in Liquid Metal Surfaces of the FNSF," *Fusion Sci. Technol.*, **75**, 918 (2019); https://doi.org/10.1080/15361055.2019.1602399
7. D. ANDRUCZYK et al., "Latest Liquid Lithium/Metal Research Results from the Center for Plasma Material Interaction," presented at 23rd Topl. Mtg. Technology of Fusion Energy (TOFE 2018), Orlando, Florida, November 11–15, 2018.
8. S. SMOLENTSEV, "A Concept of Liquid Metal Flowing First Wall and Integrated Tub-Like Divertor," presented at 23rd Topl. Mtg. Technology of Fusion Energy (TOFE 2018), Orlando, Florida, November 11–15, 2018. https://doi.org/10.1080/15361055.2019.1602399
9. M. ABDOU et al., "On the Exploration of Innovative Concepts for Fusion Chamber Technology," *Fusion Eng. Des.*, **54**, 181 (2001); https://doi.org/10.1016/S0920-3796(00)00433-6.
10. R. E. NYGREN et al., "A Fusion Reactor Design with a Liquid First Wall and Divertor," *Fusion Eng. Des.*, **72**, 181 (2004); https://doi.org/10.1016/j.fusengdes.2004.07.007.
11. Y. HIROOKA et al., "A Review of the Present Status and Future Prospects of the Application of Liquid Metals for Plasma-Facing Components in Magnetic Fusion Devices," *Fusion Sci. Technol.*, **68**, 477 (2015); https://doi.org/10.13182/FST15-125.
12. M. A. JAWORSKI, A. KHODAK, and R. KAITA, "Liquid-Metal Plasma-Facing Component Research on the National Spherical Torus Experiment," *Plasma Phys. Control. Fusion*, **55**, 124040 (2013); https://doi.org/10.1088/0741-3335/55/12/124040.
13. F. L. TABARES, "Present Status of Liquid Metal Research for a Fusion Reactor," *Plasma Phys. Control. Fusion*, **58**, 014014 (2015); https://doi.org/10.1088/0741-3335/58/1/014014.
14. M. KONDO and Y. NAKAJIMA, "Boiling Points of Liquid Breeders for Fusion Blankets," *Fusion Eng. Des.*, **88**, 2556 (2013); https://doi.org/10.1016/j.fusengdes.2013.05.049.
15. J. YIN et al., "Thermodynamic Assessment of the Li-Sn (Lithium-Tin) System," *J. Alloys Compounds*, **393**, 105 (2005); https://doi.org/10.1016/j.jallcom.2004.09.047.
16. P. HUBBERSTEY et al., "Is Pb-17Li really the eutectic alloy? A redetermination of the lead-rich section of the Pb-Li phase diagram ($0.0 < x_{Li}(at\%) < 22.1$)," *J. Nucl. Mater.*, **191–194**, 283 (1992); https://doi.org/10.1016/S0022-3115(09)80051-2.
17. J. SANGSTER and A. D. PELTON, "The Ga-Li (Gallium-Lithium) System," *J. Phase Equilibria*, **12**, 33 (1991); https://doi.org/10.1007/BF02663670.
18. W. A. ALEXANDER et al., "The Lithium-Indium System," *Can. J. Chem.*, **54**, 1052 (1976); https://doi.org/10.1139/v76-150.
19. J. P. ALLAIN, D. N. RUZIC, and M. R. HENDRICKS, "D, He and Li Sputtering of Liquid Eutectic Sn-Li," *J. Nucl. Mater.*, **290–293**, 33 (2001); https://doi.org/10.1016/S0022-3115(00)00504-3.

20. J. P. ALLAIN, D. N. RUZIC, and M. R. HENDRICKS, "Measurements and Modeling of D, He and Li Sputtering of Liquid Lithium," *J. Nucl. Mater.*, **290–293**, 180 (2001); https://doi.org/10.1016/S0022-3115(00)00508-0.

21. M. D. COVENTRY, J. P. ALLAIN, and D. N. RUZIC, "D+, He+ and H+ Sputtering of Solid and Liquid Phase Tin," *J. Nucl. Mater.*, **313–316**, 636 (2003); https://doi.org/10.1016/S0022-3115(02)01369-7.

22. R. P. DOERNER et al., "Measurements of Erosion Mechanisms from Solid and Liquid Materials in PISCES-B," *J. Nucl. Mater.*, **290–293**, 166 (2001); https://doi.org/10.1016/S0022-3115(00)00568-7.

23. R. P. DOERNER et al., "Behavior of High Temperature Liquid Surfaces in Contact with Plasma," *J. Nucl. Mater.*, **313–316**, 383 (2003); https://doi.org/10.1016/S0022-3115(02)01359-4.

24. R. P. DOERNER, S. I. KRASHENINNIKOV, and K. SCHMID, "Particle-Induced Erosion of Materials at Elevated Temperature," *J. Appl. Phys.*, **95**, 4471 (2004); https://doi.org/10.1063/1.1687038.

25. R. P. DOERNER et al., "High Temperature Erosion of Beryllium," *J. Nucl. Mater.*, **337–339**, 877 (2005); https://doi.org/10.1016/j.jnucmat.2004.09.025.

26. J. P. ALLAIN, M. D. COVENTRY, and D. N. RUZIC, "Temperature Dependence of Liquid-Lithium Sputtering from Oblique 700 eV He Ions," *J. Nucl. Mater.*, **313–316**, 641 (2003); https://doi.org/10.1016/S0022-3115(02)01371-5.

27. T. D. ROGNLIEN, M. E. RENSINK, and D. P. STOTLER, "Scrape-Off Layer Plasma and Neutral Characteristics and Their Interactions with Walls for FNSF," *Fusion Eng. Des.*, **135**, 380 (2018); https://doi.org/10.1016/j.fusengdes.2017.07.024.

28. T. D. ROGNLIEN and M. E. RENSINK, "Interactions Between Liquid-Wall Vapor and Edge Plasmas," *J. Nucl. Mater.*, **290–293**, 312 (2001); https://doi.org/10.1016/S0022-3115(00)00575-4.

29. T. ABRAMS et al., "Suppressed Gross Erosion of High-Temperature Lithium via Rapid Deuterium Implantation," *Nucl. Fusion*, **56**, 016022 (2016); https://doi.org/10.1088/0029-5515/56/1/016022.

30. D. POST et al., "Steady-State Radiative Cooling Rates for Low-Density, High-Temperature Plasmas," *At. Data Nucl. Data Tables*, **20**, 397 (1977); https://doi.org/10.1016/0092-640X(77)90026-2.

31. W.-H. SHIH and D. STROUD, "Theory of the Surface Tension of Liquid Metal Alloys," *Phys. Rev. B*, **22**, 804 (1985); https://doi.org/10.1103/PhysRevB.32.804.

32. J. LEE, W. SHIMODA, and T. TANAKA, "Surface Tension and Its Temperature Coefficient of Liquid Sn-X (X=Ag, Cu) Alloys," *Mater. Trans.*, **45**, 2864 (2004); https://doi.org/10.2320/matertrans.45.2864.

33. R. BASTASZ and J. A. WHALEY, "Surface Composition of Liquid Metals and Alloys," *Fusion Eng. Des.*, **72**, 111 (2004); https://doi.org/10.1016/j.fusengdes.2004.07.005.

34. R. BASTASZ and W. ECKSTEIN, "Plasma–Surface Interactions on Liquids," *J. Nucl. Mater.*, **290–293**, 19 (2001); https://doi.org/10.1016/S0022-3115(00)00557-2.

35. J. P. S. LOUREIRO et al., "Behavior of Liquid Li-Sn Alloy as Plasma Facing Material on ISTTOK," *Fusion Eng. Des.*, **117**, 208 (2017); https://doi.org/10.1016/j.fusengdes.2016.12.031.

36. B. B. ALCHAGIROV, F. F. DYSHEKOVA, and R. K. ARKHESTOV, "Surface Tension of Lead-Lithium Melts," *Russian J. Phys. Chem. A*, **90**, 2262 (2016); https://doi.org/10.1134/S0036024416110029.

37. V. Z. KANCHUKOEV et al., "Polytherms of Surface Tension and Density of Melts of Lead-Lithium System," *High Temp.*, **47**, 292 (2009); https://doi.org/10.1134/S0018151X09020217.

38. P. F. ADAMS et al., "Solubilities, and Solution and Solvation Enthalpies, for Nitrogen and Hydrogen in Liquid Lithium," *J. Less-Common Metals*, **42**, 325 (1975); https://doi.org/10.1016/0022-5088(75)90052-1.

39. P. HUBBERSTEY et al., "Hydrogen in Liquid Alkali Metals," *J. Less-Common Metals*, **49**, 253 (1979); https://doi.org/10.1016/0022-5088(76)90039-4.

40. E. VELECKIS, E. H. VAN DEVENTER, and M. BLANDER, "Lithium-Lithium Hydride System," *J. Phys. Chem.*, **78**, 1933 (1974); https://doi.org/10.1021/j100612a013.

41. F. J. SMITH et al., "The Solubility and Isotopic Exchange Equilibrium for Hydrogen Isotopes in Lithium," *J. Inorg. Nucl. Chem.*, **41**, 1001 (1979); https://doi.org/10.1016/0022-1902(79)80077-9.

42. H. U. BORGSTEDT and C. GUMINSKI, "IUPAC-NIST Solubility Data Series. 75. Nonmetals in Liquid Alkali Metals," *J. Phys. Chem. Ref. Data*, **30**, 846 (2001); https://doi.org/10.1063/1.1391426.

43. C. E. MESSER et al., "Solid-Liquid Equilibrium in the Lithium Lithium Hydride System," *J. Phys. Chem.*, **62**, 220 (1958); https://doi.org/10.1021/j150560a018.

44. GOLUBCHIKOV et al., "Development of a Liquid-Metal Fusion Reactor Divertor with a Capillary-Pore System," *J. Nucl. Mater.*, **233–237**, 667 (1996); https://doi.org/10.1016/S0022-3115(96)00010-4.

45. Y. NAGAYAMA, "Liquid Lithium Divertor System for Fusion Reactor," *Fusion Eng. Des.*, **84**, 1380 (2009); https://doi.org/10.1016/j.fusengdes.2009.02.002.

46. R. J. GOLDSTON, R. MYERS, and J. SCHWARTZ, "The Lithium Vapor Box Divertor," *Phys. Scr.*, **2016**, 014017 (2016); https://doi.org/10.1088/0031-8949/T167/1/014017.

47. N. EUSTATHOPOULOS, "Wetting by Liquid Metals—Application in Materials Processing: The Contribution of the Grenoble Group," *Metals*, **5**, 350 (2015); https://doi.org/10.3390/met5010350.

48. B. KOMOLAFE and M. MEDRAJ, "Progress in Wettability Study of Reactive Systems," *J. Metallurgy*, 2014, article ID 387046; https://doi.org/10.1155/2014/387046.

49. H. NAKAE, H. FUJII, and K. SATO, "Reactive Wetting of Ceramics by Liquid Metals," *Materials Trans. JIM*, **33**, 400 (1992); https://doi.org/10.2320/matertrans1989.33.400.

50. J. LUO, "A Short Review of High-Temperature Wetting and Complexion Transitions with a Critical Assessment of Their Influence on Liquid Metal Embrittlement and Corrosion," *Corrosion*, **72**, 897 (2016); https://doi.org/10.5006/1925.

51. P. FIFLIS et al., "Wetting Properties of Liquid Lithium on Select Fusion Relevant Surfaces," *Fusion Eng. Des.*, **89**, 2827 (2014); https://doi.org/10.1016/j.fusengdes.2014.03.060.

52. S. SMOLENTSEV, "MHD Duct Flows Under Hydrodynamic 'Slip' Condition," *Theor. Comput. Fluid Dyn.*, **23**, 557 (2009); https://doi.org/10.1007/s00162-009-0108-7.

53. C. CHOI and M. KIM, *Wettability Effects on Heat Transfer, Two Phase Flow, Phase Change and Numerical Modeling*, (2011), ISBN:978-953-307-584-6; http://www.intechopen.com/books/two-phase-flow-phase-change-and-numerical-modeling/wettability-effects- on-heat-transfer (current as of June 1, 2018).

54. M. HVASTA, Princeton Plasma Physics Laboratory, "Designing and Optimizing a Moving Magnet Pump for Sodium Systems," Personal Communication, 2018.

55. M. J. BALDWIN et al., "Deuterium Retention in Liquid Lithium," *Nucl. Fusion*, **42**, 305 (2002); https://doi.org/10.1088/0029-5515/42/11/305.

56. E. OYARZABAL, A. B. MARTÍN-ROJO, and F. L. TABARÉS, "Comparative Studies of H Absorption/Desorption Kinetics and Evaporation of Liquid Lithium in Different Porous Systems and Free Surfaces," *Fusion Eng. Des.*, **117**, 217 (2017); https://doi.org/10.1016/j.fusengdes.2016.08.009.

57. A. B. MARTIN-ROJO et al., "Laboratory Studies of H Retention and LiH Formation in Liquid Lithium," *Fusion Eng. Des.*, **89**, 2915 (2014); https://doi.org/10.1016/j.fusengdes.2014.07.015.

58. A. DE CASTRO et al., "Temperature Dependence of Liquid Lithium Film Formation and Deuterium Retention on Hot W Samples Studied by LID-QMS. Implications for Future Fusion Reactors," *Nucl. Fusion*, **58**, 046003 (2018); https://doi.org/10.1088/1741-4326/aaa8d0.

59. J. M. CANIK et al., "Edge Transport and Turbulence Reduction with Lithium Coated Plasma Facing Components in the National Spherical Torus Experiment," *Phys. Plasma*, **18**, 056118 (2011); https://doi.org/10.1063/1.3592519.

60. D. P. BOYLE et al., "The Relationships Between Edge Localized Modes Suppression, Pedestal Profiles and Lithium Wall Coatings in NSTX," *Plasma Phys. Control. Fusion*, **53**, 105011 (2011); https://doi.org/10.1088/0741-3335/53/10/105011.

61. J. S. HU et al., "An Overview of Lithium Experiments on HT-7 and EAST During 2012," *Fusion Eng. Des.*, **89**, 2875 (2014); https://doi.org/10.1016/j.fusengdes.2014.06.015.

62. T. H. OSBOURNE et al., "Enhanced H-Mode Pedestals with Lithium Injection in DIII-D," *Nucl. Fusion*, **55**, 063018 (2015); https://doi.org/10.1088/0029-5515/55/6/063018.

63. E. WOLFRUM et al., "Impact of Wall Materials and Seeding Gases on the Pedestal and on Core Plasma Performance," *Nucl. Mater. Energy*, **12**, 18 (2017); https://doi.org/10.1016/j.nme.2017.01.002.

64. P. S. KRSTIC et al., "Deuterium Uptake in Magnetic-Fusion Devices with Lithium-Conditioned Carbon Walls," *Phys. Rev. Lett.*, **110**, 105001 (2013); https://doi.org/10.1103/PhysRevLett.110.105001.

65. J. P. TONKS et al., "Corrosion Studies of LiH Thin Films," *J. Nucl. Mater.*, **484**, 228 (2017); https://doi.org/10.1016/j.jnucmat.2016.12.008.

66. P. F. TORTORELLI et al., "Effects of Nitrogen and Nitrogen Getters in Lithium on the Corrosion of Type 316 Stainless Steel"; https://inis.iaea.org/collection/NCLCollectionStore/_Public/10/472/10472566.pdf (Mar. 1979) (current as of June 1, 2018).

67. H. KONDO et al., "IFMIF/EVEDA Lithium Test Loop: Design and Fabrication Technology of Target Assembly as a Key Component," *Nucl. Fusion*, **51**, 123008 (2011); https://doi.org/10.1088/0029-5515/51/12/123008.

68. K. NATESAN and W. E. RUTHER, "Fabrication and Properties of a Tin–Lithium Alloy," *J. Nucl. Mater.*, **307**, 743 (2002); https://doi.org/10.1016/S0022-3115(02)01221-7.

69. J. NEUHAUSEN et al., "Mercury Purification in the MW Liquid Metal Spallation Target of EURISOL-DS"; http://www.hep.princeton.edu/mumu/target/Neuhausen/neuhausen_accapp07.pdf (current as of June 1, 2018).

70. A. DAVIS et al., "Neutronics Aspects of the FESS-FNSF," *Fusion Eng. Des.*, **135**, Part B, 271 (2018); https://doi.org/10.1016/j.fusengdes.2017.06.008.

71. M. A. FUTTERER et al., "On the Use of Tin–Lithium Alloys as Breeder Material for Blankets of Fusion Power Plants," *J. Nucl. Mater.*, **283-287**, 1375 (2000); https://doi.org/10.1016/S0022-3115(00)00124-0.

72. *Liquid Metal Handbook*, R. N. LYON, Ed., Atomic Energy Commission, Washington D.C. (1950).

73. M. KONDO, M. ISHII, and T. MUROGA, "Corrosion of Steels in Molten Gallium (Ga), Tin (Sn) and Tin Lithium Alloy (Sn–20li)," *Fusion Eng. Des.*, **98–99**, 2003 (2015); https://doi.org/10.1016/j.fusengdes.2015.05.051.

74. M. KONDO et al., "Corrosion–Erosion and Mass Transfer Dynamic Behaviors of Reduced Activation Ferritic/Martensitic Steel in a Nonisothermal Pb-17Li System," *Fusion Eng. Des.*, **136**, Part B, 1581 (2018); https://doi.org/10.1016/j.fusengdes.2018.05.062.

75. E. E. HOFFMAN and R. W. HARRISON, "The Compatibility of Refractory Metals with Liquid Metals," *Refractory Metal Alloys Metallurgy and Technology*, I. MACHLIN, Ed., American Institute of Mining, Metallurgical and Petroleum Engineers (1968).

76. J. R. DISTAFANO and E. E. HOFFMAN, "Corrosion Mechanisms in Refractory Metal—Alkali Metal Systems," Oak Ridge National Laboratory report ORNL-3424 (1963); https://www.osti.gov/scitech/servlets/purl/4635104 (current as of June 1, 2018).

77. P. F. TORTORELLI and J. M. DEVAN, "Thermal-Gradient Mass Transfer in Lithium-Stainless Steel Systems," *J. Nucl. Mater.*, **85–86**, 289 (1979); https://doi.org/10.1016/0022-3115(79)90504-X.

78. P. F. TORTORELLI and O. K. CHOPRA, "Corrosion and Compatibility Considerations of Liquid Metals for Fusion Reactor Applications," *J. Nucl. Mater.*, **103**, 621 (1981); https://doi.org/10.1016/0022-3115(82)90668-7.

79. O. K. CHOPRA and P. F. TORTORELLI, "Compatibility of Materials for Use in Liquid-Metal Blankets of Fusion Reactors," *J. Nucl. Mater.*, **123**, 1201 (1984); https://doi.org/10.1016/0022-3115(84)90241-1.

80. O. K. CHOPRA and D. L. SMITH, "Corrosion of Ferrous Alloys in a Flowing Lithium Environment," *J. Nucl. Mater.*, **133–134**, 861 (1985); https://doi.org/10.1016/0022-3115(85)90275-2.

81. K. SHIBATA et al., "Compatibility of Fusion Reactor Materials with Flowing Lithium," *J. Nucl. Mater.*, **123**, 1252 (1984); https://doi.org/10.1016/0022-3115(84)90250-2.

82. O. K. CHOPRA and D. L. SMITH, "Influence of Temperature and Lithium Purity on Corrosion of Ferrous Alloys in a Flowing Lithium Environment," *J. Nucl. Mater.*, **141–143**, 584 (1986); https://doi.org/10.1016/0022-3115(86)90058-9.

83. M. KONDO et al., "Flow Accelerated Corrosion and Erosion-Corrosion of RAFM Steel in Liquid Breeders," NIFS-993, National Institute for Fusion Studies (2012); http://www.nifs.ac.jp/report/NIFS-993.pdf. (current as of June 1, 2018).

84. J. H. DEVAN, J. E. SELLE, and A. E. MORRIS, "Review of Lithium Iron-Base Alloy Corrosion Studies," ORNL/TM-4927, Oak Ridge National Laboratory (1976); https://www.osti.gov/servlets/purl/4087807 (current as of June 1, 2018).

85. B. A. PINT, L. R. WALKER, and K. A. UNOCIC, "Material Compatibility with Isothermal Pb–Li," *Mater. High Temp.*, **29**, 129 (2012); https://doi.org/10.3184/096034012X13334529777329.

86. A. S. SREE et al., "Preliminary Corrosion Studies of IN-RAFM Steel with Stagnant Lead Lithium at 550°C" (2017) (unpublished); https://arxiv.org/pdf/1706.05000.pdf (current as of June 1, 2018).

87. M. KONDO et al., "Metallurgical Study on Corrosion of RAFM Steel JLF-1 in Pb-Li Alloys with Various Li Concentrations," *Fusion Eng. Des.*, **125**, 316 (2017); https://doi.org/10.1016/j.fusengdes.2017.04.058.

88. J. KONYS et al., "Flow Rate Dependent Corrosion Behavior of Eurofer Steel in Pb–15.7Li," *J. Nucl. Mater.*, **417**, 1191 (2011); https://doi.org/10.1016/j.jnucmat.2010.12.277.

89. J. KONYS et al., "Comparison of Corrosion Behavior of EUROFER and CLAM Steels in Flowing Pb-15.7Li," *J. Nucl. Mater.*, **455**, 491 (2014); https://doi.org/10.1016/j.jnucmat.2014.07.045.

90. W. KRAUSS, S.-E. WULF, and J. KONYS, "Long-Term Corrosion Behavior of ODS-Eurofer in Flowing Pb-15.7Li at 550°C," *Nucl. Mater. Energy*, **9**, 512 (2016); https://doi.org/10.1016/j.nme.2016.04.011.

91. E. PLANTACIS et al., "Corrosion Phenomena of Eurofer Steel in Pb-17Li Stationary Flow at Magnetic Field," *Proc. Int. Conf. Nuclear Engineering (ICONE14)*, Miami, Florida, July 17–20, 2006, ASME (2006).

92. A. S. SREE et al., "Preliminary Corrosion Studies of P-91 in Flowing Lead–Lithium with and Without Magnetic Field for Indian Lead–Lithium Ceramic Breeder Test Blanket Module," *Nucl. Fusion*, **54**, 083029 (2014); https://doi.org/10.1088/0029-5515/54/8/083029.

93. M. C. GAZQUEZ et al., "Magnetic Field Effect on the Corrosion Processes at the Eurofer-Pb-17Li Flow Interface," *J. Nucl. Mater.*, **465**, 633 (2015); https://doi.org/10.1016/j.jnucmat.2015.06.024.

94. A. HEINZEL, A. WEISENBURGER, and G. MÜLLER, "Corrosion Behavior of Austenitic Steel AISI 316L in Liquid Tin in the Temperature Range Between 280 and 700 °C," *Mater. Corros.*, **68**, 831 (2017); https://doi.org/10.1002/maco.v68.8.

95. A. R. PETROVA et al., "The Selection of Materials Resistant to Molten Tin at High Temperature," *Met. Sci. Heat Treat.*, **11**, 819 (1969); https://doi.org/10.1007/BF00652062.

96. B. A. PINT et al., "Development of ODS FeCrAl for Compatibility in Fusion and Fission Energy Applications," *JOM*, **68**, 2458 (2014); https://doi.org/10.1007/s11837-014-1200-z.

97. S. MAJUMDAR et al., "Formation of Al_2O_3/FeAl Coatings on a 9Cr-1Mo Steel, and Corrosion Evaluation in Flowing Pb-17Li Loop," *J. Nucl. Mater.*, **486**, 60 (2017); https://doi.org/10.1016/j.jnucmat.2017.01.021.

98. F. BARBIER and J. BLANC, "Corrosion of Martensitic and Austenitic Steels in Liquid Gallium," *J. Mater. Res.*, **14**, 737 (1999); https://doi.org/10.1557/JMR.1999.0099.

99. H. KAMDAR, "Embrittlement by Liquid Metals," *Treatise on Materials Science and Technology*, Vol. 25, p. 361, Elsevier (1983).

100. W. ROSTOKER, J. M. McCAUGHEY, and H. MARKUS, *Embrittlement by Liquid Metals*, Reinhold Publishing Corporation, New York (1960).

101. M. G. NICHOLAS and C. F. OLD, "Liquid Metal Embrittlement," *J. Mater. Sci.*, **14**, 1 (1979); https://doi.org/10.1007/BF01028323.

102. S. G. KELLER and A. P. GORDON, "Experimental Study of Liquid Metal Embrittlement for the Aluminum 7075–Mercury Couple," *Eng. Fract. Mech.*, **84**, 146 (2012); https://doi.org/10.1016/j.engfracmech.2012.02.005.

103. J. C. HIRVONEN et al., "Use of Liquid Metal Embrittlement for Controlled Fracture," ARL-TR-4976, Army Research Laboratory (Sep. 2009).

104. J. ZHANG, P. HOSEMANN, and S. MALOY, "Models of Liquid Metal Corrosion," *J. Nucl. Mater.*, **404**, 82 (2010); https://doi.org/10.1016/j.jnucmat.2010.05.024.

105. I. LYUBLINSKI, S. MIRNOV, and V. LAZAREV, "Protection of Tokamak Plasma Facing Components by a Capillary Porous System with Lithium," *J. Nucl. Mater.*, **463**, 1156 (2015); https://doi.org/10.1016/j.jnucmat.2014.12.017.

106. R. VISWANATHSAN et al., "Materials Technology for Advanced Coal Power Plants," U.S. Department of Energy/Ohio Coal Research Office; https://www.phase-trans.msm.cam.ac.uk/2005/LINK/188.pdf (current as of June 1, 2018).

107. G. MAZZITELLI et al., "Experiments on FTU with an Actively Water Cooled Liquid Lithium Limiter," *J. Nucl. Mater.*, **463**, 1152 (2015); https://doi.org/10.1016/j.jnucmat.2014.12.050.

108. P. RINDT et al., "Conceptual Design of a Pre-Loaded Liquid Lithium Divertor Target for NSTX-U," *Fusion Eng. Des.*, **112**, 204 (2016); https://doi.org/10.1016/j.fusengdes.2016.08.020.

109. M. S. TILLACK et al., "Design and Analysis of the ARIES-ACT1 Fusion Power Core," *Fusion Sci. Technol.*, **67**, 49 (2015); https://doi.org/10.13182/FST14-790.

110. X. WANG et al., "ARIES-ACT2 DCLL Power Core Design and Engineering," *Fusion Sci. Technol.*, **67**, 193 (2015); https://doi.org/10.13182/FST14-798.

111. J. A. TEPROVICH Jr. et al., "Electrochemical Extraction of Hydrogen Isotopes from Li/LiT Mixtures," *Fusion Eng. Des.*, **139**, 1 (2019); https://doi.org/10.1016/j.fusengdes.2018.11.018.

112. A. HASSANEIN, "Modeling Hydrogen and Helium Entrapment in Flowing Liquid Metal Surfaces as Plasma-Facing Components in Fusion Devices," *J. Nucl. Mater.*, **302**, 41 (2002); https://doi.org/10.1016/S0022-3115(02)00726-2.

113. M. NIETO et al., "Helium Retention and Diffusivity in Flowing Liquid Lithium," *J. Nucl. Mater.*, **313–316**, 646 (2003); https://doi.org/10.1016/S0022-3115(02)01372-7.

114. C. E. KESSEL et al., "Core Plasma Physics Basis and Its Impacts on the FNSF," *Fusion Eng. Des.*, **135**, Part B, 356 (2018); https://doi.org/10.1016/j.fusengdes.2017.06.003.

115. H. KATSUDA et al., "Conceptual Design of the IFMIF Target Facility," *Fusion Sci. Technol.*, **30**, 1152 (1996); https://doi.org/10.13182/FST96-A11963104.

116. P. HUMRICKHOUSE and B. J. MERRILL, "Tritium Aspects of the Fusion Nuclear Science Facility," *Fusion Eng. Des.*, **135**, Part B, 302 (2018); https://doi.org/10.1016/j.fusengdes.2017.04.099.

117. V. A. EVTIKHIN et al., "Energy Removal and MHD Performance of Lithium Capillary-Pore Systems for Divertor Target Application," *Fusion Eng. Des.*, **49–50**, 195 (2000); https://doi.org/10.1016/S0920-3796(00)00423-3.

118. S. V. MIRNOV et al., "Li-CPS Limiter in Tokamak T-11M," *Fusion Eng. Des.*, **65**, 455 (2003); https://doi.org/10.1016/S0920-3796(03)00018-8.

119. M. A. JAWORSKI, A. KHODAK, and R. KAITA, "Liquid-Metal Plasma-Facing Component Research on the National Spherical Torus Experiment," *Plasma Phys. Control. Fusion*, **55**, 124040 (2013); https://doi.org/10.1088/0741-3335/55/12/124040.

120. M. SHIMADA and Y. HIROOKA, "Actively Convected Liquid Metal Divertor," *Nucl. Fusion*, **54**, 122002 (2014); https://doi.org/10.1088/0029-5515/54/12/122002.

121. N. B. MORLEY et al., "Experimental Investigation of Free Liquid Metal Jets in Vacuum: Preliminary Results for IFE Chamber Wall Protection Applications," *Fusion Sci. Technol.*, **34**, 1035 (1998); https://doi.org/10.13182/FST98-A11963750.

122. S. V. MIRNOV, V. N. DEM'YANENKO, and E. V. MURAV'EV, "Liquid-Metal Tokamak Divertors," *J. Nucl. Mater.*, **196–198**, 45 (1992); https://doi.org/10.1016/S0022-3115(06)80010-3.

123. R. MOIR, "Jets and Droplets Compared to a Moving Slab of Liquid for Divertor Cooling for a Tokamak Magnetic Fusion Energy Reactor," Vallecitos Molten Salt Research Associates (2008); http://www.ralphmoir.com/wp-content/uploads/2012/10/jetdrop_0317081.pdf (current as of June 1, 2018).

124. J. MIYAZAWA et al., "Conceptual Design of a Liquid Metal Limiter/Divertor System for the FFHR-d1," *Fusion Eng. Des.*, **125**, 227 (2017); https://doi.org/10.1016/j.fusengdes.2017.07.003.

125. A. YING et al., "Exploratory Studies of Flowing Liquid Metal Divertor Options for Fusion-Relevant Magnetic Fields in the MTOR Facility," *Fusion Eng. Des.*, **72**, 35 (2004); https://doi.org/10.1016/j.fusengdes.2004.07.004.

126. M. D. NORNBERG et al., "A Liquid Metal Flume for Free Surface Magnetohydrodynamic Experiments," *Rev. Sci. Instrum.*, **79**, 094501 (2008); https://doi.org/10.1063/1.2976109.